The interaction of Escherichia coli O157:H7 and Salmonella Typhimurium flagella with host cell membranes and cytoskeletal components

Eliza B Wolfson, Johanna Elvidge, Amin Tahoun, Trudi Gillespie, Judith Mantell, Sean P Mcateer, Yannick Rossez, Edith Paxton, Fiona Lane, Darren J Shaw, et al.

MICROBIOLOGY

RESEARCH ARTICLE

Wolfson *et al.*, *Microbiology*

DOI 10.1099/mic.0.000959

MICROBIOLOGY SOCIETY

OPEN MICROBIOLOGY

The interaction of *Escherichia coli* O157:H7 and *Salmonella* Typhimurium flagella with host cell membranes and cytoskeletal components

Eliza B. Wolfson[1,2,*], Johanna Elvidge[1], Amin Tahoun[1,3], Trudi Gillespie[4]†, Judith Mantell[2], Sean P. McAteer[1], Yannick Rossez[5], Edith Paxton[1], Fiona Lane[6], Darren J. Shaw[7], Andrew C. Gill[6], Jo Stevens[1], Paul Verkade[2], Ariel Blocker[8], Arvind Mahajan[1] and David L. Gally[1,*]

Abstract

Bacterial flagella have many established roles beyond swimming motility. Despite clear evidence of flagella-dependent adherence, the specificity of the ligands and mechanisms of binding are still debated. In this study, the molecular basis of *Escherichia coli* O157:H7 and *Salmonella enterica* serovar Typhimurium flagella binding to epithelial cell cultures was investigated. Flagella interactions with host cell surfaces were intimate and crossed cellular boundaries as demarcated by actin and membrane labelling. Scanning electron microscopy revealed flagella disappearing into cellular surfaces and transmission electron microscopy of *S.* Typhiumurium indicated host membrane deformation and disruption in proximity to flagella. Motor mutants of *E. coli* O157:H7 and *S.* Typhimurium caused reduced haemolysis compared to wild-type, indicating that membrane disruption was in part due to flagella rotation. Flagella from *E. coli* O157 (H7), EPEC O127 (H6) and *S.* Typhimurium (P1 and P2 flagella) were shown to bind to purified intracellular components of the actin cytoskeleton and directly increase *in vitro* actin polymerization rates. We propose that flagella interactions with host cell membranes and cytoskeletal components may help prime intimate attachment and invasion for *E. coli* O157:H7 and *S.* Typhimurium, respectively.

INTRODUCTION

Bacterial flagella are macromolecular machines predominately associated with movement toward preferred environmental niches [1]. They are composed of a long, hollow, capped filament of polymeric flagellin, connected to a flagella basal body through a hook complex [2]. The basal body houses a motor complex that rotates the basal body rod, hook and semi-rigid helical flagella filament, or flagellum, to move the bacterium [3, 4]. The basal body also contains an adapted type 3 secretion export system that regulates secretion of the different components during flagellum assembly [5, 6]. Flagellin monomers make up the majority of the flagellum and have a hairpin-like structure with highly conserved associating termini and central variable domains [7]. *Salmonella enterica* serovar Typhimurium can alternately express two flagella types, presumably to help avoid the adaptive immune response; phase 1 (P1)

Received 14 April 2020; Accepted 13 July 2020; Published 04 September 2020

Author affiliations: [1]Division of Immunity and Infection, The Roslin Institute and R(D)SVS, The University of Edinburgh, Easter Bush, Midlothian, EH25 9RG, UK; [2]Departments of Biochemistry, Biomedical Sciences Building, The University of Bristol, Bristol, BS8 1TD, UK; [3]Faculty of Veterinary Medicine, Kafrelsheikh University, 33516 Kafr el-Sheikh, Egypt; [4]IMPACT Facility, Centre for Integrative Physiology, University of Edinburgh, Edinburgh, EH8 9XD, UK; [5]Génie Enzymatique et Cellulaire, UMR 7025 CNRS, Centre de recherche Royallieu, Sorbonne Universités, Université de Technologie de Compiègne, Compiègne Cedex, France; [6]Division of Neurobiology, The Roslin Institute and R(D)SVS, The University of Edinburgh, Easter Bush, Midlothian, EH25 9RG, UK; [7]Division of Clinical Sciences, The Roslin Institute and R(D)SVS, The University of Edinburgh, Easter Bush, Midlothian, EH25 9RG, UK; [8]Department of Cellular and Molecular Medicine, Biomedical Sciences Building, The University of Bristol, Bristol, BS8 1TD, UK.

***Correspondence:** Eliza B. Wolfson, elizawolfson@gmail.com; David L. Gally, david.gally@roslin.ed.ac.uk

Keywords: adherence; actin; cytoskeleton; *Escherichia coli*; flagella; membrane; *Salmonella*.

Abbreviations: CFL1, cofilin-1; DMEM, Dulbecco's minimal essential medium; EBL, embryonic bovine lung; FCS, foetal calf serum; GAL4, galectin-4; GFP, green fluorescent protein; HBSS, Hank's balanced salt solution; HEK293, human embryonic kidney 293 cells; IPEC-J2, intestinal porcine epithelial cells - J2; LB, lysogeny broth; LEE, locus of enterocyte effacement; MAMP, microbe-associated molecular pattern; MEM-HEPES, minimal essential medium buffered with N-2-hydroxyethylpiperazine-N-ethanesulfonic acid; mot, motor; NLRC4, NOD-like and CARD domain-containing receptor 4; P1, phase-1 flagellin (FliC); P2, phase-2 flagellin (FljB); PBS, phosphate-buffered saline; RBC, red blood cells; RT, room temperature; SCV, Salmonella-containing vacuole; SEM, scanning electron microscopy; TLR5, Toll-like receptor 5; T3SS, type-3 secretion system; Tx100, Triton X-100.

†Deceased

Three supplementary tables, three supplementary figures and four supplementary movies are available with the online version of this article.

flagella are composed of FliC flagellin, and phase 2 (P2) flagella are composed of FljB flagellin [8]. In the stacked flagella filament, the flagellin region exposed on the surface shows little conservation between strains and is used for immunological serotyping, resulting in the H-type. The flagellin termini are stacked inside the filament and drive flagellin polymerization [9]. These more conserved and buried regions are important microbe-associated molecular patterns (MAMPs), which activate Toll-like receptor 5 (TLR5) and NOD-like and CARD domain-containing receptor 4 (NLRC4) [10–13].

In peritrichous and monotrichous species, flagella have been shown to sense surfaces and cause a switch from motile to sessile lifestyles, making flagellar adhesion the preliminary step essential for bacterial colonization [14]. More recently, flagellar rotation has been shown to play a role in flagella adherence, surface stiffness sensing and inducing neutrophil extracellular traps [15, 16]. However, mechanistic information beyond near-surface swimming [17] is lacking and direct adherence along the filament shaft to cell surface components is poorly defined.

Important zoonotic enteropathogens, enterohaemorrhagic *Escherichia coli* O157:H7 and *S.* Typhimurium both express flagella and type 3 secretion systems (T3SSs), but have different intestinal colonization strategies. T3SSs are structurally related to the flagella basal body and act as molecular needles to inject effector proteins into host cells [18]. *E. coli* O157:H7 use their T3SSs to inject effector proteins into host intestinal epithelial cells, inducing actin polymerization and the formation of attaching and effacing lesions [19]. This cytoskeletal network modulation allows *E. coli* O157:H7 to bind very tightly to the surface of host enterocytes while avoiding phagocytosis [20, 21]. In contrast to *E. coli* O157:H7, *S.* Typhimurium translocates T3SS effectors into host epithelial cells, leading to changes in the actin cytoskeleton that promote bacterial invasion [22]. *Salmonella* survival in host cells requires a second T3SS, which manipulates host cell responses and the position and recognition of the *Salmonella* containing vacuole (SCV) [23]. *E. coli* O157:H7 is mainly an extracellular bacterium, but is reliant on both a T3SS and its H7 flagella for cell binding and colonization of its reservoir host, cattle [24–26]. Published studies indicate that H7 flagella bind to mucus and more recent work demonstrated binding of different *E. coli* flagella, including H7, to ionic phospho- and sulpho-lipids [27, 28]. In contrast, *S.* Typhimurium is invasive in humans and animals, including cattle and pigs, with invasion being dependent on two different T3SSs [29]. However, the significance of flagella expression by *S.* Typhimurium for initial attachment and the identity of potential protein ligands remain inconclusive [30–32].

This study takes a closer look at the molecular basis of bacterial flagella adherence to host cells in the context of pathogenic colonization. We start by looking at actin associated with bacterial flagella when bacteria are in contact with host cells. We observe deformation and possible disruption of host plasma membranes in proximity to flagella and explore the possible consequences if membranes are breached by flagella. Actin and flagella interactions are confirmed by pull-downs, far-Western blotting and *in vitro* actin polymerization assays. These data shed some light on the interactions between the flagella of *E. coli* O157:H7 and *S.* Typhimurium and host cells, including membrane and cytoskeletal components, that may prime the next steps in the infection process.

METHODS

Bacterial strains and growth conditions

Bacterial strains (Table 1) were stored as saturated cultures in lysogeny broth (LB) with 25% glycerol at −70 °C. Bacteria were grown in LB at 28–30 °C (*E. coli* O157:H7) or 37 °C (*S.* Typhimurium) at 200 r.p.m. The antibiotics, when required, were chloramphenicol or kanamycin at 50 μg ml^{-1} and ampicillin at 100 μg ml^{-1}. To assess strain motility, fresh colonies were stab-inoculated once into 0.3% (w/v) LB agar. Inoculated plates were incubated at room temperature (RT) for 36 h. Assays were carried out in quadruplicate from separate colonies.

Mutant strain construction

The flagellin gene *fliC*$_{H7}$ from the *E. coli* O157:H7 strain TUV93-0 was exchanged with *fliC*$_{H6}$ according to the allelic exchange method published by Blomfield *et al.* [33]. Briefly, homologous recombination of pEBW6 or pEBW7 (Table S1, available in the online version of this article) with TUVΔ*fliC* (Table 1) and counter-selection of *sacB* with sucrose was used to generate TUVΔ*fliC* chromosomally complemented with *fliC*$_{H6}$ (*TUVfliC*$_{H6F}$) and *fliC*$_{H7}$ (TUV*fliC*$_{H7F}$), respectively. Strains were validated by PCR with *sacB*, *fliC* locus and O157 specific primer pairs (Table S2), Sanger sequencing, motility in 0.3% (w/v) LB agar and wide-field fluorescence microscopy of saturated cultures with 1:1000 dilutions of H6- and H7- specific rabbit IgG (Table S3). The TUV93-0 *motA* mutant (ZAP1575, Table 1) was constructed by allelic exchange using pTOF25*motA* (Table S1) and primer sets: No-motA, Ni-motA, Co-motA and Ci-motA (Table S2). The deleted region corresponds to 2653444–2654278 of EDL933 and was verified by sequencing. A chromosomally complemented strain was made (ZAP1576, Table 1) using the amplicon of primers No-motA/Co-motA (Table S2) and cloning and exchange with the resultant pTOF25 construct. This *motA* complemented version of ZAP1575 has restored motility (Fig. S3). P22 transduction of phase-locked (*hin*) and *motA* mutations into the SL1344 background from the LT2 strains (Table 1) was carried out using standard transduction protocols from strains used and verified in previous studies (Table 1).

Antibodies and purified proteins

Abbreviations and/or Uniprot accession codes are in parentheses. The sources, details and use of antibodies and stains are described in Table S3. Rabbit skeletal muscle αβ-actin

Table 1. Strains used or constructed in this study

Strain	Relevant features	Source
TUV93-0	*E.coli* O157:H7; EDL933 (ATCC 700927) *stx*$^{-}$	[67]
TUVΔ*fliC*	TUV93-0 *fliC*::*sacB*::*kan*^{r}, aflagellate	[28]
TUV*fliC*$^{-}$	TUV93-0 *fliC*$^{-}$, aflagellate	[28]
TUV$fliC_{H7F}$	TUVΔ*fliC cis* complement $fliC_{H7}$ from TUV93-0	This study
TUV$fliC_{H6F}$	TUVΔ*fliC cis* complement $fliC_{H6}$ from E2348/69	This study
ZAP1574	TUV93-0 Δ*motA*	This study
ZAP1575	TUV93-0 *motA*$^{-}$	This study
ZAP1576	TUV93-0 *motA*-complemented	This study
ZAP734	*E. coli* O157:H7 NCTC 12900, Stx^{-}	AHVLA
E2348/69	*E. coli* O127:H6; sequenced	[68]
MG1655	*E. coli* K12; sequenced	[69]
TUV Δ*LEE1-2*	8.9 Kb deletion in LEE1-3, ETTA1	[70]
SL1344	*S.* Typhiumurium	[71]
SL1344Δ$fljB_{P2}$	SL1344 Δ*fljB* by λred, expresses only P1	[71]
SL1344Δ$fliC_{P1}$	SL1344 Δ*fliC* by λred, expresses only P2	[71]
SL1344 Δ$fliC_{P1}$ Δ$fljB_{P2}$	SL1344 Δ*fliC* and Δ*fljB* by λred, aflagellate	[71]
ZAP1566	*S.* Typhiumurium LT2 *fliM*5978-GFP *motAB*::Tc^{R}, non-motile	P. Aldridge Lab, Newcastle
SL1344Δ*motAB*	SL1344 P22 transduced with ZAP1566, non-motile	This study
Maskan	*S.* Typhimurium	Stock from Lohmann Animal Health
4/74	*S.* Typhimurium	[72]
4/74 *prgH*$^{-}$	*prgH*::mini-Tn 5Km2 mutant of ST4/74 Nal^{R}	[73]

(ACTB, P29751), human platelet βγ-actin (ACTB, P60709), recombinant human cofilin-1 (CFL1 P23528) and arp2/3 complex (ARPC4 Q148J6) from bovine brain were all purchased from Cytoskeleton, Inc. Recombinant human galectin-4 (GAL4 P56470) and gelsolin (GSN Q3S×14) from bovine plasma were purchased from R&D Systems and Sigma, respectively.

Flagella were sheared from the mutants TUV$fliC_{H7F}$ (H7, Q7DBI0), TUV$fliC_{H6F}$ (H6, B7USU2), *TUVfliC*$^{-}$::pEW5 (H48, P04949), *SL1344*Δ$fljB_{P2}$ (phase-1, P1, FliC E1WGJ5) and SL1344Δ$fliC_{P1}$ (P2, FljB E1WA22), using an adapted protocol [34]. TUV93-0 derivatives were cultured at 30 °C and SL1344 derivatives at 37 °C. Briefly, strains were cultured on 0.3% (w/v) LB agar for 24 h. LB was inoculated with 10 µl agar plugs from the leading edge of the motility halo and incubated at 200 r.p.m for 16 h. For purification of H48 flagella, *TUVfliC*$^{-}$::pEW5 was grown in the presence of ampicillin at all times. *TUVfliC*$^{-}$::pEW5 was further sub-cultured in LB in the same conditions to OD_{600} 0.6, at which point 1 mM IPTG was added and cultures were then grown to OD_{600} 1–1.5. All cultures were centrifuged at 4100 ***g*** at 4 °C for 30 min and pellets were resuspended 1:10 initial culture volume with cold Dulbecco A phosphate-buffered saline (PBS). These were then sheared for 2 min on ice with at maximum speed with an IKA T-10 homogenizer (Ultra-Turrax). Two to five rounds of centrifugation at 4100 ***g*** at 4 °C for 15 min, followed by centrifugation once at 16000 ***g*** at 4 °C for 10 min, were undertaken to obtain bacteria-free supernatants. These were centrifuged at 145000 ***g*** 4 °C for 1.5 h and resuspended in PBS (or 50 mM Tris/HCl pH 7.5 for actin polymerization assays) at 1:500 of initial culture volumes. Protein concentration and purity was assessed using BCA, and then confirmed by Coomassie staining (Imperial protein stain, Thermo Fisher) and densitometry after SDS-PAGE.

Sheared flagella were monomerized according to the protocol published by Smith *et al.* [35]. Flagella preparations were incubated at 70 °C for 15 min and then filtered by centrifugation at 5000 ***g*** at 4 °C for 30 min using 100 kDa 4 ml filter units (Millipore). Filtrates were confirmed by size-exclusion HPLC to be exclusively monomeric.

Tissue culture

All cells were maintained at 37 °C in 5% CO_2 and at 80% humidity. The embryonic bovine lung epithelial

(EBL; laboratory stocks), murine fibroblast (3T3; laboratory stocks) and HEK293 (laboratory stocks) cell lines were maintained in Dulbecco's minimal essential medium (DMEM; Sigma) supplemented with 10% (v/v) foetal bovine serum (FBS; Sigma), 1 U of penicillin (Invitrogen), 1 μg ml^{-1} of streptomycin (Invitrogen) and 2 mM L-glutamine (Invitrogen), unless otherwise stated. The porcine intestinal epithelial cell line IPEC-J2 was maintained as described by Schierack *et al.* [36] in HAMS/F-12 1:1 with 5% FBS, 1 U of penicillin and 1 μg ml^{-1} of streptomycin. Prior to bacterial infection, cultured cells were washed in MEM/HEPES and incubated at 37 °C, 5% CO2, 80% humidity for 1–2 h. All bacterial infections were incubated in these conditions for the time specified unless otherwise stated.

Primary cell culture

Bovine rectal and porcine colonic epithelia were isolated from abattoir-derived tissue as described previously [37]. The intestinal tissues were collected from material discarded as part of the normal work of the abattoir; while no licence was required for this, the relevant permissions were obtained from the West Lothian abattoir. The mucosal scrapings from bovine terminal rectal or porcine colonic tissue from a local abattoir were digested in DMEM [1% (v/v) foetal calf serum (FCS), 100 U ml^{-1} penicillin, 30 μg ml^{-1} streptomycin, 25 μg ml^{-1} gentamicin] containing 75 U ml^{-1} collagenase and 20 μg ml^{-1} dispase (Roche) with gentle shaking at 37 °C until isolated crypts could be observed microscopically. Crypt enrichment from undigested contaminating gut microflora and single cells including fibroblasts was performed using a series of differential centrifugation steps with DMEM containing 2% (w/v) sorbitol. Approximately 500–700 crypts were seeded per well on to collagen (Nutacon for bovine cultures, Porcogen for porcine cultures) coated plates. The bovine cells were grown for 5 days before use, and the porcine cells were grown to a stage of confluence (approximately 3×10^5 cells per well, typically at 10–14 days following initial primary epithelial cell culture).

Confocal microscopy

Unless otherwise stated, all samples for confocal microscopy outlined below were washed three times in PBS, fixed for >20 min at RT in 4% (w/v) paraformaldehyde and then permeabilized for <1 min with 0.1% (v/v) Triton X-100 prior to immediate washing as above and staining as below. All stains and antibodies were diluted in PBS. Where stained, cell nuclei were stained with DAPI (Table S3), and slides or coverslips were mounted with ProLong Gold (Invitrogen) unless otherwise stated. Image data were acquired with a Zeiss Plan Apochromat 1.4 NA ×63 oil immersion lens and a multi-track (sequential scan) experimental set-up on a Zeiss LSM510, using Axiovision software, unless otherwise stated.

For the examination of H7 flagella interactions with actin, primary bovine rectal epithelial and EBL cells were used. For primary epithelial interactions, bovine crypts isolated from rectal epithelia were seeded onto collagen-coated four-well Thermanox chamber slides as described (see primary cell culture section). Infection was for 1 h with 1×10^7 *E. coli* O157:H7 TUV93-0 grown at 28 °C 200 r.p.m, sub-cultured to OD_{600} 0.3–0.4 and resuspended in MEM/HEPES. These were then fixed, permeabilized and stained as described below, except that primary antibodies were labelled with FITC-conjugated α-rabbit IgG (Sigma). F-actin was then stained with Texas red-conjugated phalloidin diluted 1:250, after which cell nuclei were stained with DAPI diluted 1:1000.

Where EBL cells were used, they were seeded onto glass coverslips 24 h prior to infection with exponential-phase *E. coli* O157:H7 TUV93-0. TUV93-0 was grown in 0.3% (w/v) LB agar, sub-cultured into LB at 30 °C for 16 h 200 r.p.m, and then sub-cultured 1:100 in MEM/HEPES supplemented with 250 nm Fe^{2+} and 0.2% (w/v) glucose at 37 °C to an OD_{600} 0.3. EBL cells were infected with TUV93-0 at a multiplicity of infection (m.o.i.) of 20 for 3 h. Samples were treated with α-H7 rabbit IgG diluted 1:100, then α-O157 mouse IgG diluted 1:1000, followed by a co-incubation of Alexa $Fluor_{568}$-conjugated α-rabbit IgG and Alexa $Fluor_{568}$ α-mouse IgG, both diluted 1:1000. F-actin was stained with FITC-conjugated phalloidin (Molecular Probes) diluted 1:100 for 2 h. The cell nuclei were stained with DAPI diluted 1:5000.

For the investigation of *S.* Typhimurium flagella interactions with host epithelia, confluent IPEC-J2 monolayers on glass coverslips were washed three times with MEM/HEPES immediately prior to infection with *S.* Typhimurium SL1344. Bacterial cultures were incubated in LB with 300 mM NaCl at 37 °C 200 r.p.m for 16 h and then diluted to an OD_{600} of 0.3 in MEM/HEPES. IPEC-J2 cells were infected at an m.o.i. of 20 for 20 min. Samples were fixed with 2% (w/v) PFA for 20 min and then permeabilized with 0.2% (v/v) triton X-100 for 5 min. Samples were treated with P1- or P2-specific rabbit IgG (α-Hi diluted 1:100 and α-H2 diluted 1:500, respectively) and then α-O4 rabbit IgG diluted 1:500. This was then labelled with FITC-conjugated α-rabbit IgG diluted 1:1000. F-actin was stained with Texas red-conjugated phalloidin diluted 1:500 and slides were mounted in VectorShield (Vector Labs). Membrane staining of *S.* Typhimurium-infected cells was undertaken in the same way, except that cells were infected for 10 min before fixation, and prior to permeabilization, membranes were stained with Texas red-conjugated wheat-germ agglutinin diluted 1:1000 for 2 h [38]. Additionally, instead of Texas red-conjugated phalloidin, F-actin was stained with Alexa $Fluor_{647}$-conjugated phalloidin.

For the investigation of H7 flagella interactions with host cell membranes, HEK293 cells were transfected with a CRD–STREX–GFP construct that leads to fluorescent staining on the inner side of the plasma membrane [39]. Briefly, 5×10^4 HEK293 cells were seeded onto glass coverslips in DMEM with 10% (v/v) FBS, 100 U ml^{-1} penicillin and 30 μg ml^{-1} streptomycin, and cultured to 40–70% confluence. One hundred and fifty nanograms of CRD–STREX–GFP plasmid was diluted in proprietary EC buffer (Qiagen) and enhancer was added to it at 1:125 (μl ng^{-1} DNA) and incubated for 5 min at RT. Effectene (Qiagen) was added at a 3:1 ratio to the enhancer and incubated for 10 min at RT. HEK293 cells

were washed with PBS and fresh maintenance medium was added. The DNA–Effectene mixture was diluted 1:5 in maintenance medium and added to cells 1:2. Protein expression was determined 24 h post-transfection using GFP expression as a read-out. These cells were infected with *E. coli* O157:H7 TUV93-0 for 90 min. Fixed then permeabilized samples were labelled with α-H7 rabbit IgG then α-O157 rabbit IgG (Table S3) diluted 1:1000 and 1:100, respectively. Primary antibodies were labelled with Alexa $Fluor_{568}$-conjugated α-rabbit IgG diluted 1:1000. Volumetric 3D reconstructions of deconvolved images were undertaken using Volocity Visualization software version 6.3.

For all of the above confocal microscopy, image data were acquired at optimal z-slice sampling rates as determined by Zeiss software, with a 1024×1024 pixel image size. Image data were deconvolved using Huygens software (Scientific Volume Imaging, Netherlands). Deconvolved models of image data were analysed and reslices of z-stacks, montages and projection views were created using NIH ImageJ software, with final figures assembled in Adobe Photoshop CS5 and CS6. Co-incidence analysis was undertaken using the 24 October 2004 version of an open-source co-localization plug-in downloadable from http://rsbweb.nih.gov/ij/plugins/colocalisation.html. Threshold values were set based on z-stack histograms to determine the Gaussian curve of background readings for each channel, and co-incidence was output at a display value of 150. Display values were designated co-incident, not co-localized, as total co-localization was <50%.

For pre-/post-permeabilization labelling, collagen (rat tail type 1, Sigma)-coated coverslips were coated in 35% (v/v) ethanol for 4 h at 37 °C, washed in PBS and then media, and then seeded with IPEC-J2 cells for *Salmonella* infection and EBL cells for *E. coli* O157:H7 infection 24 h prior to infection. Cells at 50–80% confluence were washed with PBS and then incubated with MEM/HEPES for 1–2 h prior to infection with 1×10^7 cells of mid-exponential phase *S.* Typhimurium SL1344::pAJR145 (constitutively expressing eGFP) for 20 min, or *E. coli* O157:H7 TUV93-0::pAJR145 (constitutively expressing eGFP) for 1 h, respectively. Once infections had taken place, cells were fixed in 4% (v/v) PFA in PBS for 20 min RT°C and blocked with 3% (w/v) BSA (PBS). All incubations were for 1 h, static, in the dark and at RT. All washes and reagents were diluted in PBS alone, and washed three times with PBS between steps. Flagella were labelled 1:500 with α-P1+P2 and α-H7 polyclonal rabbit IgG (Table S3) for SL1344 and TUV93-0 infections, respectively, and then labelled 1:1000 with TRITC-conjugated α-rabbit IgG, before washing and permeabilization with 0.1% (v/v) TX100 for 30 s. Flagella labelling was then repeated as above, but with FITC-conjugated α-rabbit IgG, followed by staining with Alexa $Fluor_{647}$-conjugated phalloidin (Invitrogen, 1:125 for 20 min). Coverslips were mounted and images acquired using a Leica HCX Plan Apochromat 1.4 NA ×100 oil immersion lens in a multi-track (sequential scan) experimental set-up on a Leica SP5II confocal laser scanning microscope with Leica Application Suite X software.

Correlative transmission electron tomography

IPEC-J2 cells were seeded in rat-tail type I collagen(Sigma)-coated glass-bottomed 35 mm µ-Dishes etched with four reference grids (IBIDI) 24 h before infection with *S.* Typhimurium SL1344::pAJR145 (constitutively expressing eGFP) in the conditions stated for pre- and post-permeabilization labelling experiments. After 20 min infection in the above conditions, cells were washed three times in PBS and fixed in 4% (w/v) PFA. Cells were labelled 1:500 with α-FliC rabbit polyclonal IgG and then 1:1000 with FITC-conjugated α-rabbit IgG (Table S3). Dishes were not mounted but instead imaged in PBS using a Leica SP5II confocal laser scanning microscope to determine the locations of cell-associated flagellated bacteria on the four reference grids.

Cells were fixed and embedded in preparation for electron tomography as follows. All wash steps and treatments were diluted in ddH_2O, unless otherwise stated. Fixation was undertaken in 2.5% (w/v) glutaraldehyde (100 mM sodium cacolydate pH 7.2) for 20 min and then washed three times before post-fixing with 1% (w/v) osmium tetroxide for 20 min. After a further three washes, cells were then stained with 3% (w/v) uranyl acetate for 20 min and washed three more times. Cells were then dehydrated with graded ethanol washes for 5 min each at 70, 80, 90, 96 and 100% (v/v) before the addition of 1:1 epon epoxy resin for 1 h 30 min, with rocking, for embedding. Embedded samples were then baked at 200 °C for 5 days before removal from glass dishes with snap-freeze/thawing. The reference grids on the remaining resin were then mounted onto stubs, trimmed to areas of interest determined by confocal microscopy (see also Olmos *et al.* [40]), and cut into 300 nm thick sections using a Leica EM UC7 with an IC80HD camera. Serial sections of areas of interest were placed onto film-coated copper slot grids (Agar Scientific) and further stained with 3% (w/v) uranyl acetate for 20 min to enhance contrast before imaging. Washed grids were labelled with 15 nm gold particles both to the top and bottom of sections for 5 min and then blotted dry.

Samples were mapped to determine the location of flagellated and cell-associated bacteria using a FEI 120kV BioTwin Spirit transmission electron microscope (TEM). The TEM tilt series (from −60° to +60 in 1.5° increments) were acquired using a FEI 200kV twin lens scanning transmission electron microscope and Xplore3D software (FEI). The tilt series were reconstructed into electron tomograms using the standard workflow of IMOD and 3dMOD software packages (Boulder Laboratory for 3D EM of Cells, University of Colorado, USA) and then analysed and presented using Amira 6.0.0, where an anisotropic diffusion filter was applied to the data, and FIJI software.

Immuno-gold staining and scanning electron microscopy (SEM)

The ultra-structural details of flagella interaction with specified epithelial cell types were visualized using Hitachi 4700 Field Emission Scanning Electron microscope. The specimens were fixed in 3% gluteraldehyde in 100 mM sodium cacodylate

buffer (pH 7.4) and processed without permeabilization for SEM as described previously [37]. Immuno-gold labelling was visualized by detecting back-scattered electrons; overlays of back scattering and secondary electrons were false-coloured in Adobe Photoshop CS4 for contrast.

Haemolysis assays

All bacterial cultures were inoculated with agar plugs from the leading edge of the motility halo of fresh motility plates of the strains indicated. These cultures were incubated statically in LB at RT for 16 h. Cultures were adjusted to equal OD_{600} before addition to a V-bottomed 96-well plate at 1:1 (50 µl each) with 50% (v/v) washed sheep red blood cells (RBCs; Oxoid) in PBS. The bacteria were driven into contact with the RBCs by centrifugation at 2000 ***g*** for 5 min RT, followed by gentle mixing by pipetting. Plates were incubated 37 °C 2 h. Samples were diluted 1:1.5 with 150 µl PBS and then gently mixed by pipetting. Plates were then centrifuged 2000 ***g*** for 10 min RT to pellet RBCs. The A_{405} of 100 µl of supernatants was then measured as a read-out of total haem release. Independent replicates were undertaken three–five times, with three–four technical replicates. The mean level of haem release caused by incubation with LB alone was subtracted and data were normalized as a percentage of wild-type haem release. After tests for equal variance were performed on raw data for each strain set in Minitab 17, and homoscedastic two-tailed *t*-tests were performed on the raw data, between mutant and wild-type strains.

Preparation of cell lysates

Bovine primary rectal epithelial cells were harvested by washing twice in PBS followed by incubation with TripLE Express (Gibco) at 37 °C, 5% CO_2, 80% humidity for 10 min. An equal volume of PBS was added and then cells were scraped off, collected and centrifuged at 300 ***g*** for 2 min at RT. Cells were washed twice by resuspending cell pellets and centrifuging in PBS or Hank's balanced salt solution (HBSS). The cell pellet was resuspended in PBS or HBSS, subjected to five cycles of snap-freezing in ethanol and dry-ice and thawing at RT, and clarified by centrifugation at 18000 ***g*** for 10 min at 4 °C.

Western and far-Western blotting

Eighty micrograms of primary epithelial cell lysates or 1 µg purified receptor candidates separated in SDS-PAGE gels were Western-blotted onto nitrocellulose (Amersham, GE Healthcare) with Schaeffer–Nielsen buffer [48 mM Tris, 39 mM glycine, 20% (v/v) methanol, 0.04% (v/v) SDS, pH 9.2], at 15V for 30–60 min. Blots were blocked in Carbofree (Vector Labs) or 0.1% (v/v) $Tween_{20}$ (Sigma) in PBS (PBST) with 5% (w/v) skimmed milk powder (Sigma, Marvel) at RT for 2 h or 4 °C for 16 h. Blots were washed three times between all subsequent steps in PBST alone for 15 min at RT, with rocking. For both Western and far-Western blots, antibodies were diluted in 1% (w/v) skimmed milk powder in PBST and incubated with blots for 1 h, with rocking at RT.

Prior to antibody labelling, far-Western blots were first probed with 1 µg ml^{-1} H7 flagella in PBS for 3 h, with rocking at RT. H7 flagella were then treated with α-H7 rabbit IgG diluted 1:1000, and this was labelled with horseradish peroxidase (HRP)-conjugated α-rabbit IgG diluted 1:1000. Western blots of cell lysates were probed with α-cofilin-1 mouse IgG diluted 1:500 or α-galectin-4 goat IgG diluted 1:1000, and then a 1:1000 dilution of HRP-conjugated α-mouse or goat IgG, respectively. Blots were then developed using Pico-West SuperSignal ECL reagents (Thermo Fisher) in a G:box (Syngene), and captured using GeneSnap (Syngene).

Pull-down assays

Cyanogen bromide (CnBr)-activated sepharose 4B lyophilized beads (GE Healthcare) were used according to manufacturer's instructions. Fifty micrograms of H7 flagella was added 2:1 to CnBr beads for 16 h at 4 °C, with rocking, in coupling buffer (100 mM $NaHCO_3$ pH 8.3 containing 500 mM NaCl). Excess H7 flagella were washed off beads by five cycles of centrifugation at 18000 ***g*** for 30 s followed by resuspension of beads in equal volumes of coupling buffer. Following one additional centrifugation as above, beads were resuspended in blocking buffer (100 mM Tris/HCl, 500 mM NaCl, pH 8.0) and incubated for 2 h statically at RT. CnBr beads were then washed 10 times by centrifugation as above, with alternate cycles of suspension in coupling buffer or wash buffer (100 mM acetic acid, 100 mM sodium acetate, 500 mM NaCl, pH 4.0). On the final centrifugation, beads were suspended in 180 µg BTRE freeze-thawed cell lysate in HBSS and incubated for 16 h at 4 °C, with rocking.

CnBr beads were centrifuged at 18 000 ***g*** for 30 s and then washed by three cycles of centrifugation as above followed by resuspension in 0.1% (v/v) PBST. Beads were centrifuged as above and eluted by incubation in 2× SDS-PAGE sample buffer (Sigma) for 5 min at 100 °C and centrifuged as above. Eluted proteins were then analysed by 12% SDS-PAGE and Imperial protein staining (Thermo Fisher). Bands visible only in the presence of H7 flagella-coated CnBr beads were considered to be likely ligand candidates and equivalent cell lysate bands were excised and identified by mass spectrometry.

Mass spectrometry

Mass spectrometry, tandem mass spectrometry and peptide mass fingerprinting were undertaken by Kevin McLean at the Moredun Research Institute Proteomics Facility, UK. Protein bands from Imperial protein-stained SDS-PAGE gels were excised and delivered to the proteomics facility. Here they were trypsinized, enriched and cleaned up, and matrix-assisted laser desorption/ionization time-of-flight tandem mass spectrometry (MALDI-TOF MS/MS) was performed on a Bruker UltraflexII according to the established protocols. Spectra were then input into MASCOT peptide mass fingerprinting software (Matrix Science) as monoisotopic 1+ (*m/z*) ratios using a±50 p.p.m. tolerance to generate protein identities.

Accurate MW determination of H6, H7, H48, P1 and P2 was undertaken with online HPLC-MS in the proteomics and metabolomics facilities at the Roslin Institute, UK. Samples of sheared flagella were diluted to ~1 pmol μl^{-1} in 0.1% (v/v) formic acid and ~20 pmol was applied to a microbore HPLC column (Dionex Acclaim C18, 4.6 mm i.d., 150 mm length, 5 µm beads, 120 Å pore size) pre-equilibrated with 0.1% (v/v) formic acid by use of a Ultimate HPLC system (Dionex). Bound components were eluted with a gradient of 0.1% (v/v) formic acid in acetonitrile into the electrospray source of an amaZon ETD ion trap mass spectrometer (Bruker Daltonics, Germany). The mass spectrometer acquired full-scan mass spectra with the final spectra being an average of eight trap fills with a maximum averaging time of 200 ms. Signals corresponding to intact flagellin were summed, the raw data were smoothed and the background was subtracted, and then deconvolution was performed using the Bruker proprietary algorithm.

Enzyme-linked immunosorbent assays (ELISAs)

One microgram per well of 95% pure human platelet βγ-actin, recombinant human galectin-4 and recombinant human cofilin-1 were adsorbed to 96-well Nunc Maxisorb plates in 100 mM sodium bicarbonate pH 9.6 for 16 h at 4 °C. Wells were blocked using Carbo-free (VectorLabs) for 2 h, at RT, before washing. All wash steps involved washing three times in PBST (0.1% $Tween_{20}$). Polymers and monomers of each flagella type (as verified by size-exclusion chromatography) were diluted in PBS only at 1000, 500, 100 and 0 ng per well, in specific wells, for 3 h, before washing. Antibodies were diluted in PBST and incubated in wells for 1 h, before washing. H6, H7, P1 and P2 flagella-specific rabbit IgG (α-H6 and α-H7 1:1000; α-Hi 1:100; α-H2 1:500, respectively, Table S3), followed by HRP-conjugated α-rabbit IgG, were used to label flagella-specific binding.

Flagella binding was detected using Pico-West SuperSignal ECL reagents (Thermo Fisher) in a G:Box using GeneSnap (Syngene) at a fixed distance of 575 mm. Densitometry on wells was performed in GeneTools (Syngene), using a fixed spot radius of 25. Data were normalized according to the formula: relative binding=$10\times[(test-C^{-})/(\bar{x}\ C^{+}-C^{-})]$, where C^{-}=0 ng flagella protein, C^{+}=positive detection control. This normalization takes into account background from antibodies and assay-to-assay variation. In addition to this, no primary antibody and no ligand coating qualitative controls were performed.

Statistical analysis was carried out in R on $\log_{10}$ data from four independent experiments. Data residuals were assessed for normality using a normality plot. As it was not biologically appropriate to compare different flagella types or ligand types statistically, separate linear mixed effects models of relative binding were used to assess the statistical significance of each flagella type binding to each ligand candidate (galectin-4, cofilin-1 and actin). Flagella concentration (1000, 500, 100 ng/well) and polymerization status (polymer and monomer) were fixed effects and experiment was a random effect. Pairwise comparisons of the interaction between polymerization statuses for each flagella type in each model were then performed on the data. To correct for the large number of comparisons, an alpha level of $P<0.01$ was taken as significant.

Actin polymerization assays

Actin polymerization assays were carried out as described by Sitthidet *et al.* with minor modifications [41] and informed by Van Troys *et al.* [42]. G-actin was prepared by resuspending lyophilized pyrene-conjugated rabbit skeletal muscle αβ-actin in G-buffer (10 mM Tris/HCl, 200 µm $CaCl_2$, 200 µm ATP, 1 mM DTT, pH 7.5) for 1 h on ice, in the dark. This was then centrifuged at 100000 ***g*** for 2 h at 4 °C. The top 80% supernatant was kept on ice in the dark. Test proteins were resuspended as purified or dialyzed with U-tube concentrators (Novagen) into 50 mM Tris/HCl pH 7.5. Molar concentrations of all protein components were calculated using a Bradford assay with a BSA standard curve. Densitometry of Coomassie-stained SDS-PAGE gels was used to adjust flagella values.

Assays were carried out in black opaque 96-well plates (Nunc). First, 1 µm actin was added to wells with 50 mM Tris/HCl pH 7.5. Cofilin-1 and serially diluted flagella preparations were then added, followed by polymerization buffer (at a final concentration of 5 mM KCl, 0.2 mM $MgCl_2$ and 0.1 mM ATP). Samples were excited at 365 nm, and emission data were measured at 407 nm for 1 h, at 30 s intervals. A daily gain value was applied to all wells to normalize actin polymerization capability and this was calculated using pyrene-actin fluorescence after 1 h polymerization at RT as above.

The maximum velocity (V_{max}) of actin polymerization was calculated using the formula $V_{max}=(A_2-A_1)/(T_2-T_1)$, where A=absorbance at 407 nm and T=time. Differences due to the addition of flagella were assessed for statistical significance using GLMs in Minitab 16.2.4. In these models, V_{max} was the response and replicate was a random factor. With flagella titration experiments, GLM analysis was carried out on data from five independent experiments; flagella type and concentration were fixed factors. Post-hoc Tukey pairwise comparisons of the interaction between flagella type and concentration were carried out. With flagella±cofilin-1 experiments, GLM analysis was carried out on data from three independent experiments; flagella type and cofilin-1 concentration were fixed factors. Post-hoc Tukey pairwise comparisons of the interaction between cofilin-1 concentration and flagella type were carried out as a very conservative estimate of differences based on the set of assumptions in a GLM statistical model. Therefore, if P values are <0.05, they are very likely to be valid and so were taken as statistically significant.

Size-exclusion chromatography

Samples were applied to an HPLC column (Sigma TSK G4000SWXL, 4.6 mm i.d., 300 mm length, 8 µm beads, 450 Å pore size) pre-equilibrated with 100 mM Tris/HCl, 200 mM NaCl, 1 mM DTT, pH 8.0, by use of an Ultimate HPLC system (Dionex), measuring absorbance at 220 nm. Columns were

calibrated by the maximum peak of elution of individual molecular weight standards: blue dextran (2.5 MDa) at ~5 ml, BSA (66 kDa) at ~10 ml, and ribonuclease A (13.5 kDa) and ATP (0.5 Da) at ~12 ml.

For verification of flagellin polymerization status, polymeric and monomeric H6, H7, H48, P1 and P2 flagellin purified into 50 mM Tris/HCl pH 7.5 were applied neat to the column three times at 30 min intervals, with three blank runs in between flagella types. Data were analysed by establishing the lowest value of all runs as a baseline and calculating the area under curve (AUC) for each run, and looking at the ratio of filaments (4.5–9 ml ≈>2 MDa–~300 kDa) to monomers (9–11.25 ml <~300 kDa) with the formula AUC=$[(A_1+A_2)/2] \times(T_2-T_1)$, where A=absorbance at 220 nm and T=time (ml).

RESULTS

Bacterial flagella labelling can be coincident with host F-actin staining

In experimental systems that allow bacteria to come into contact with host cells without centrifugation, co-incidence of flagella and F-actin labelling was routinely detected, 60 min post-infection for *E. coli* O157:H7 (Figs 1, S1 and Movie S1) and 20 min post-infection for *S.* Typhimurium (Fig. 1c). For *Salmonella,* co-incidence of flagella with F-actin staining raised the possibility that flagella were not necessarily confined to the *Salmonella* containing vacuole (SCV) during invasion. It was also possible to observe flagella expressed by extracellular *Salmonella* co-incident with actin at early infection time points. However, not all flagella that were imaged (bacterially associated or not) were found to be coincident with phalloidin-stained actin (Fig. 1d). Where flagella were coincident with F-actin staining, this followed a striated pattern, consistent with the helical wave of flagella filaments.

Bacterial flagella labelling is intermittently masked by membranes

Coincidence of bacterial flagella with F-actin staining (Fig. 1) was detected after samples were fixed with 4% (w/v) PFA and then permeabilized with 0.1% (w/v) Triton X-100 (Tx100). Depending on the level of proximity of bacterial flagella to cortical actin, this could involve some contact with the plasma membrane. Biological membranes are sensitive to non-ionic detergents such as Tx100. To observe whether Tx100 treatment altered flagella labelling, confocal microscopy was carried out on GFP-expressing *E. coli* O157:H7 and *S.* Typhimurium SL1344-colonized epithelial cells. Cells were fixed and then flagella were labelled with specific antibodies before (red) and after (green) Tx100 treatment. F-actin was then labelled with Alexa $Fluor_{647}$ phalloidin (blue, see the Methods section). Cell-associated flagellated *S.* Typhimurium and *E. coli* O157:H7 were imaged in 3D stacks and representative projections are presented in Fig. 2. Pre-permeabilization staining of flagella was often interrupted or less intense in short portions of the flagella, where post-permeabilization staining of the same flagella was comparatively even (Fig. 2). This indicates that bacterial flagella were intermittently masked by a detergent-sensitive component, such as a membrane, during the initial stages of infection.

Bacterial flagella are detectable on both sides of host cell membranes

To investigate how close flagella associations with host cell surfaces might be, flagellated adherent *E. coli* O157:H7 and *S.* Typhimurium were imaged in the context of plasma membrane labelling. For *E. coli* O157:H7 infections, HEK293 cells were transiently transfected with a trans-membrane voltage-gated ion channel fusion protein. This ion channel contains a green fluorescent protein (GFP) in the C-terminal cytoplasmic domain. The fluorescent signal generated reports the position of the internal cytoplasmic face of the plasma membrane only [39]. H7 flagella were imaged passing in and out of the GFP-labelled cytoplasmic face of the plasma membrane (Fig. 3a, c). Volumetric 3D reconstruction of the labelling in these confocal microscopy images allowed the visualization of transverse sections, showing H7 flagella labelling within the cell cytoplasmic boundaries (Fig. 3b, d).

In contrast, wheat germ agglutinin binds to the external sugar-coated surface of epithelial cell membranes [38]. Confocal microscopy of eukaryotic plasma membranes, labelled with fluorescent wheat germ agglutinin after *S.* Typhimurium infection but before fixation, revealed flagella bundles of invasive *S.* Typhimurium passing through regions of plasma membrane staining (Fig. 3e). Flagella were observed passing both from inside-to-outside and outside-to-inside host cell areas. Both *E. coli* O157:H7 and *S.* Typhimurium flagella were observed passing through gross cellular boundaries by confocal microscopy.

Defining bacterial flagella interactions with host cell membranes by electron microscopy

The z-plane resolution limit of confocal laser scanning microscopy is ~500 nm with the fluorophores used, but host cell plasma membranes are only ~5 nm thick. O157:H7 immunogold SEM was used to take a closer look at H7 flagella interactions with host cell surfaces without Tx100 treatment. As with confocal microscopy of pre-permeabilization labelling, *E. coli* O157:H7 flagella immune-gold staining was interrupted as the filament disappeared at the primary intestinal epithelial cell surface, and then resumed as it curled upwards away from the surface (Fig. 4a, b). SEM of *S.* Typhimurium at early time points of infection (10–30 min, again without Tx100 treatment) also revealed flagella-like filaments interacting intimately with cell surfaces of primary intestinal epithelial cells (Fig. 4c). These filaments could be seen disappearing and reappearing at the cell surface, consistent with the actin coincidence observed by confocal microscopy. *S.* Typhimurium flagella-like filaments were also observed associating with membrane ruffles and protrusions during the invasion process (Fig. 4d, e).

These observations were made with serologically and structurally distinct flagella (Fig. S2), hinting that a biophysical mechanism may be involved. To look for evidence of

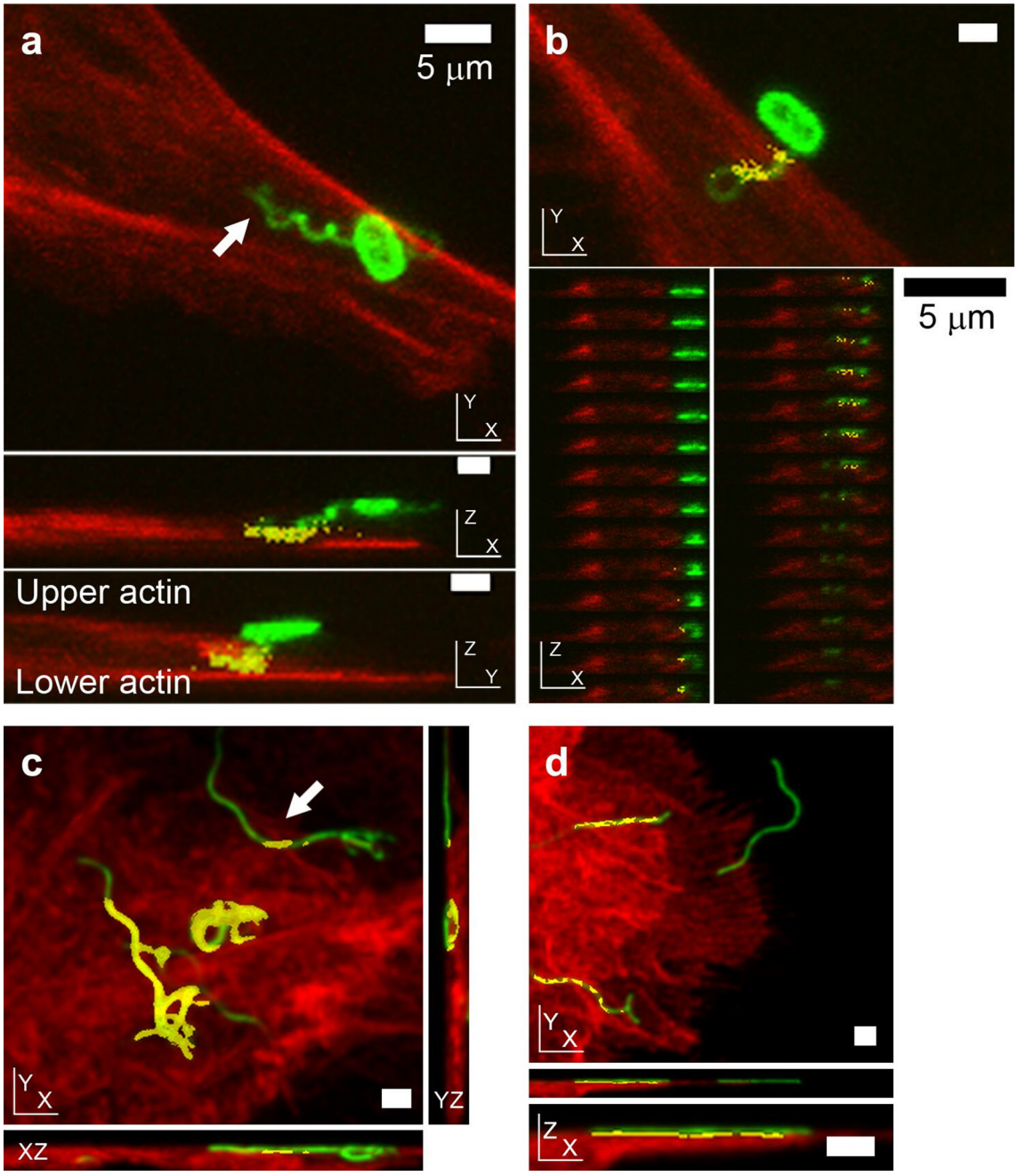

Fig. 1. Position of *E. coli* O157:H7 and *S.* Typhimurium flagella relative to host cell F-actin during early colonization, as determined by confocal microscopy. Phalloidin-labelled actin is red, antibody-labelled LPS and flagella are green, and coincidence of the two is yellow. (a, b) Confocal micrographs of *E. coli* O157:H7 (TUV93-0) interacting with primary bovine epithelial cell cultures 1 h post-infection. (a) Interaction of *E. coli* O157:H7 with host actin with its H7 flagellum in XY, XZ and YZ projections (3D rotating image in Movie S1, individual Z-slices of XZ and YZ projections are presented in Fig. S1). (b) Co-incidence of phalloidin-stained actin with an *E. coli* O157-associated coiled H7 flagellum, but not with the bacterium itself, by XY projection, with individual XZ slices shown beneath. (c, d) Confocal micrographs of O4:P2 stained *S.* Typhimurium (SL1344) interacting with IPEC-J2 cells 20 min post-infection. (c) XY and orthogonal projections of a 3D micrograph where a flagellum emanating from a non-invasive bacterium coincident with actin staining is indicated by an arrow. (d) XY projection of a 3D confocal micrograph of P2 flagella (green) adhering to the cell surface. Not all P2 flagella are coincident with actin, but where there is co-incidence, it is periodic. All samples were fixed with 4% (w/v) paraformaldehyde for >20 min prior to permeabilization. Scale bars, 1 μm unless indicated otherwise.

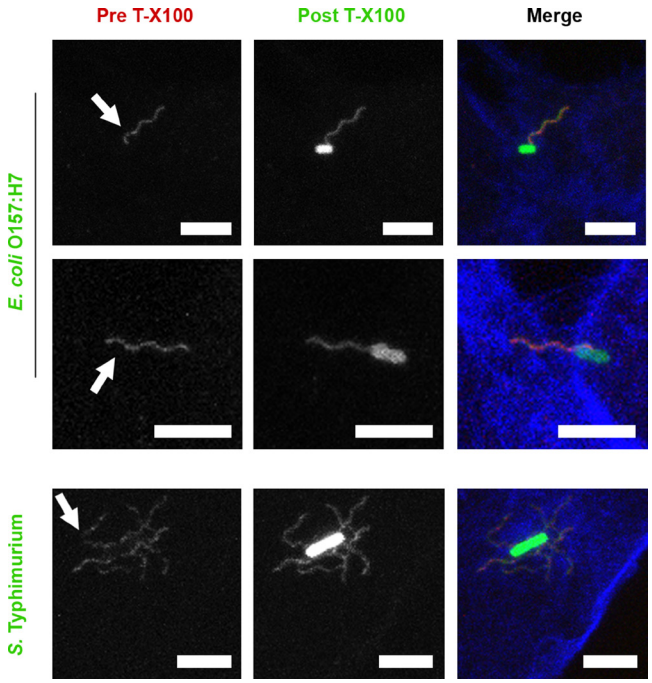

Fig. 2. Confocal microscopy of *E. coli* O157:H7 and *S.* Typhimurium flagella staining before and after Triton X-100 treatment. *E. coli* O157:H7 TUV93-0::pAJR145 (constitutively expressing GFP) interacting with EBL cells for 1 h, and *S.* Typhimurium SL1344::pAJR145 interacting with IPEC-J2 epithelial cells for 20 min before fixation with 4% (w/v) paraformaldehyde for >20 min. Prior to permeabilization, flagella were labelled with antibodies (red). After permeabilization with 0.1% (v/v) Triton X-100 for 30 s, flagella were labelled with antibodies again (green). Cells were labelled with phalloidin-Alexa Fluor$_{647}$ (blue). Scale bars, 5 µm.

biophysical interactions of flagella with host cell membranes, *S.* Typhimurium flagella closely associated with host cells were located with correlative light and electron microscopy and examined by thick-section transmission electron tomography (Fig. 5). To preserve the details and visibility of the host cell membranes, conventional post-section staining of flagella was not undertaken, but the visibility of the structures in the tomogram slices was enhanced by applying an anisotropic diffusion filter and a blue–orange ICB colour lookup table in Amira software.

Host cell membranes were observed encapsulating bundles of flagella filaments during the *S.* Typhimurium invasion process (Fig. 5a, b, Movies S2 and S3). Consistent with previous microscopy, these flagella were located within gross cellular boundaries at points, but they were separated from the host cytosol by deformed but contiguous host membranes. Visually distinct from these observations was the reduction or interruption of clear membrane staining in proximity to bacterial flagella (Fig. 5c, Movie S4). In this example, the flagella filaments are largely accessible to extracellular antibody labelling, as shown by the punctae that occur regularly along their length. Fig. 5c2 shows the labelled bundle of flagella filaments drawing close to a clearly defined plasma membrane, but as they come into presumable contact, the membrane boundary is both deformed and less distinct, and in places apparently absent.

Bacteria with paralysed flagella cause less membrane disruption

To test whether flagella rotation is even capable of causing physical disruption of host cell membranes, sheep RBCs were used as a model dye-filled eukaryotic plasma membrane, as they contain haem pigment. Short-term incubation of RBCs was undertaken with bacteria and their isogenic flagella and flagella motor (*mot)* mutants; *mot* mutants result in the production of full-length flagella that do not rotate. Bacteria were cultured under conditions known to induce expression of flagella and briefly centrifuged into contact with RBCs to eliminate the contribution of motility and chemotaxis to this process (Fig. 6; see the Methods section).

All flagellate wild-type strains caused membrane disruption upon interaction with RBCs, as determined by haem release. As haem release could be due to the T3SSs of either pathogen, T3SS mutants (ΔprgH for *S.* Typhimurium, ΔLEE1-2 for *E. coli* O157:H7; Table 1) were tested under these flagella-selective growth conditions (Fig. 6). Mutation of T3SSs resulted in altered mean levels of haem release compared to wild-type for both *S.* Typhimurium (~30% reduction) and *E. coli* O157:H7 (~10% increase). Both effects were statistically significant (P<0.0001 and 0.0039, respectively), suggesting that the T3SSs were directly involved in haem release.

Mutation of flagella and flagella rotation caused reduced mean levels of haem release for both *S.* Typhimurium and *E. coli* O157:H7. For *S.* Typhimurium, the levels of haem release were approximately half that of the wild-type in both flagellin (Δ*fliC*Δ*fljB*) and motility (Δ*motAB*) mutants, with statistically significant values (P<0.0001 for both; Fig. 6). For wild-type *E. coli* O157:H7, mean levels of haem release were much less affected by flagellin (*fliC*$^-$) and motor (*motA*$^-$) mutation. Reductions of ~5% for *fliC*$^-$ were not statistically significant (P=0.17). In contrast, a reduction of ~10% for *motA*$^-$ was statistically significant (P=0.0046). The subtle effect for *E. coli* O157:H7 may reflect the lower overall flagella expression and the lower rotation speeds and motility of *E. coli* wild-type compared to *Salmonella* (Fig. S3 [43, 44]). We infer from these results that the flagella of *S.* Typhimurium and *E. coli* O157:H7 are physically able to disrupt eukaryotic plasma membranes and flagellar rotation is likely to play a role.

Bacterial flagella can interact with components of the actin cytoskeleton *in vitro*

If bacterial flagella can disrupt host cell membranes, perhaps they are also able to interact with cytosolic components just beneath host cell membranes. Initial pull-downs and far-Western blotting with H7 flagella identified β-actin (ACTB1), cofilin-1 (CFL1) and galectin-4 (GAL4) as potential interactants (Fig. S4). A 'far' ELISA was designed to assess relative flagella binding to human βγ-actin, recombinant human CFL1 and recombinant human GAL4. These purified proteins

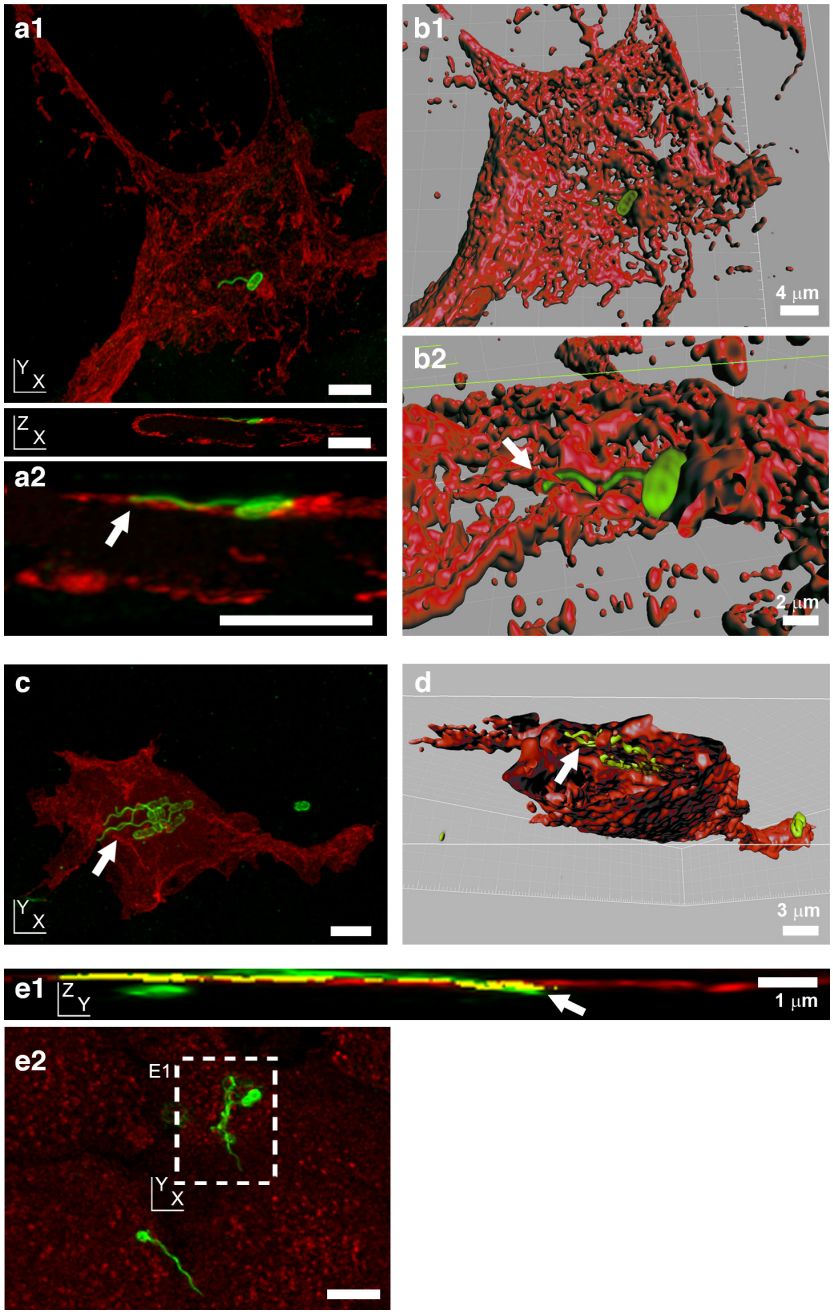

Fig. 3. Position of *E. coli* O157:H7 and *S.* Typhimurium flagella relative to host cell membranes, as determined by confocal microscopy. (a, c) Projections of 3D confocal micrographs of *E. coli* O157:H7 (TUV93-0: LPS and flagella are green) interacting with HEK293 cells transiently transfected with a transmembrane protein–fluorescent protein fusion construct (red, see the Methods section) 1.5 h post-infection. This transfection causes labelling of the cytoplasmic face of the plasma membrane cytosolic leaflet [39]. (b, d) 3D volume-rendered model of images in (a) and (c), respectively, using Volocity Visualization software. Arrows indicate intracellular flagella. (a1) XY and XZ projections of a single flagellum emanating from a bacterium on a transfected HEK293 cell, 3D-rendered in (b1) and enlarged in (a2). A similar view has been 3D-rendered in (b2), where the arrow indicates intracellular flagella. (c) XY projection of the binding of a cluster of bacteria expressing H7 flagella to a transfected HEK293 cell. (d) Transverse cut-through of the HEK293 cell, with flagella visible beneath the layer defined by the cytoplasmic staining of the labelled ion channel protein (arrow). (e) Projections of a 3D confocal micrograph of O4:P2 stained *S.* Typhimurium SL1344 (green) interacting with wheat germ agglutinin-labelled IPEC-J2 cells (red) 10 min post-infection. This labelling stains N-acetylglucosamine and sialic acid moieties on the external face of cell membranes [38]. (e1) YZ projection of the XY inset labelled in (e2), with a long flagella bundle that passes out then back into the cell (arrow). Coincidence of flagella and membrane staining is shown in yellow. (e2) XY projection of whole image shown in (e1). All samples were fixed in 4% (w/v) para-formaldehyde for >20 min prior to permeabilization. Scale bars, 5 µm unless indicated otherwise.

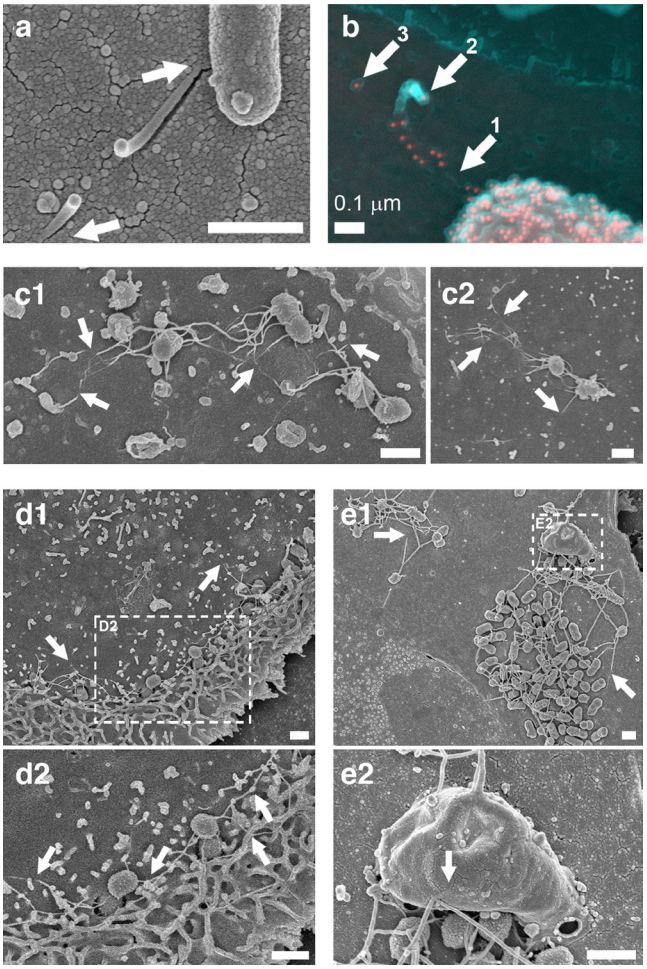

Fig. 4. SEM of *E. coli* O157:H7 and *S.* Typhimurium flagella-like structures disappearing and reappearing at host cell surfaces. (a, b) *E. coli* O157 : H7 (ZAP734) interactions with bovine primary epithelial cell cultures 3 h post-infection. (a) Secondary electron (SE) image of a snapped flagella-like filament, which appears to penetrate the cell surface (arrows). (b) A false-coloured SE image (cyan) superimposed with a false-coloured back-scattered image (red). H7 flagella and O157 LPS are both immuno-gold labelled. Filament staining occurs adjacent to the bacterium and is then absent (arrow 1). The filament is then broken and curls back on itself (arrow 2), with the remnant embedded filament (arrow 3). (c1, c2) SE images of flagella-like filaments disappearing into and coming out of the surface of IPEC-J2 epithelial cells (arrows) within the first 30 min of infection with *S.* Typhimurium (Maskan). (d) SE image of *S.* Typhimurium (Maskan) micro-colonies on IPEC-J2 cells 40 min post-infection. (d1) Actin ruffling proximal to invading *Salmonella*. (d2) Enlarged from the inset indicated in (d1). Wavy flagella-like filaments are interacting with ruffled and unruffled cell surfaces (arrows). (e) SE image of *S.* Typhimurium SL1344 (WT) micro-colonies on bovine primary epithelial cells. (e1) Long filaments disappearing into the cell surface (arrows). (e2) Higher resolution image of the area indicated in (b1), which shows long filaments interacting with a large macropinocytic protrusion (arrow). Samples were fixed in 3% (w/v) glutaraldehyde and were not permeabilized prior to sample processing for SEM. Imaging was undertaken on a Hitachi 4700 field emission scanning electron microscope. Scale bars, 1 μm unless indicated otherwise.

were coated to 96-well plates and probed with 1000–100 ng flagellins, and then binding was detected using appropriate antibodies. Binding data were normalized to negative (no flagellin added) and positive (wells coated with 1 μg flagellin) detection controls to give a measure of relative binding (see the Methods section). Binding of polymeric and monomeric flagellin from *E. coli* O127:H6, *E. coli* O157:H7, commensal *E. coli* K12:O175:H48 and *S.* Typhimurium O4:Hi/H2 expressing either P1 or P2 flagella was assessed (Figs 7 and S2).

For all interactions tested, except for H48-CFL1 (P=0.55), monomeric flagellins bound at significantly lower levels than polymeric flagellins (Fig. 7, P=0.0023–0.0001 or less, depending on the flagellin tested), serving as a suitable baseline for non-binding in this assay. This was particularly the case for the actin interactions, where binding by flagellin monomers was virtually undetectable in this assay for each flagellin type tested.

There were different patterns of binding between *E. coli* and *S.* Typhimurium polymeric flagellins; *E. coli* flagellins showed higher relative binding to CFL1 compared to βγ-actin under these conditions, and conversely the *S.* Typhimurium flagellins tested showed a stronger association with βγ-actin, compared to CFL1. All polymeric flagellins tested bound to GAL4, although there was no particular distinction between *S.* Typhimurium and *E. coli* relative levels. Binding to GAL4 was not a consequence of flagella post-translational glycosylation; determination of molecular weights by mass spectrometry of H6 and H7 sheared preparations indicated that these flagellins were unmodified, whilst modified forms of *S.* Typhimurium flagellins were consistent with methylation (data not shown [45]).

Bacterial flagella can increase actin polymerization rates *in vitro*

To further confirm the *in vitro* binding interactions of H6, H7, P1 and P2 polymeric flagellin with actin, their effect on actin polymerization was assessed (Fig. 8a). We used 1 mM pyrene-conjugated rabbit αβ-actin in 10 mM Tris/HCl, 200 μm $CaCl_2$, 200 μm ATP, 1 mM DTT, pH 7.5 as a baseline (actin control). Actin polymerization was initiated by the addition of final concentrations of 5 mM KCl, 0.2 mM $MgCl_2$ and 0.1 mM ATP (actin). The actin-severing activity of CFL1 at 2:1 ratio with actin generates more rapidly polymerizing 'plus' ends of actin [46], so 500 nM CFL1 was added as a positive control for enhanced rates of actin polymerization (cofilin-1). The bacterial flagella filaments tested all enhanced *in vitro* rabbit αβ-actin polymerization to variable extents, implying a direct interaction with physiologically active actin (Fig. 8a). Higher median actin polymerization V_{max} rates were determined for all flagella tested when compared to actin alone, with P2 flagella showing a statistically significant dose-dependent effect (P=0.003, Fig 8a, b).

To investigate whether H6 and H7 flagella interactions with CFL1 enhanced the effect they had on actin polymerization, αβ-actin was co-incubated with the four flagella types and

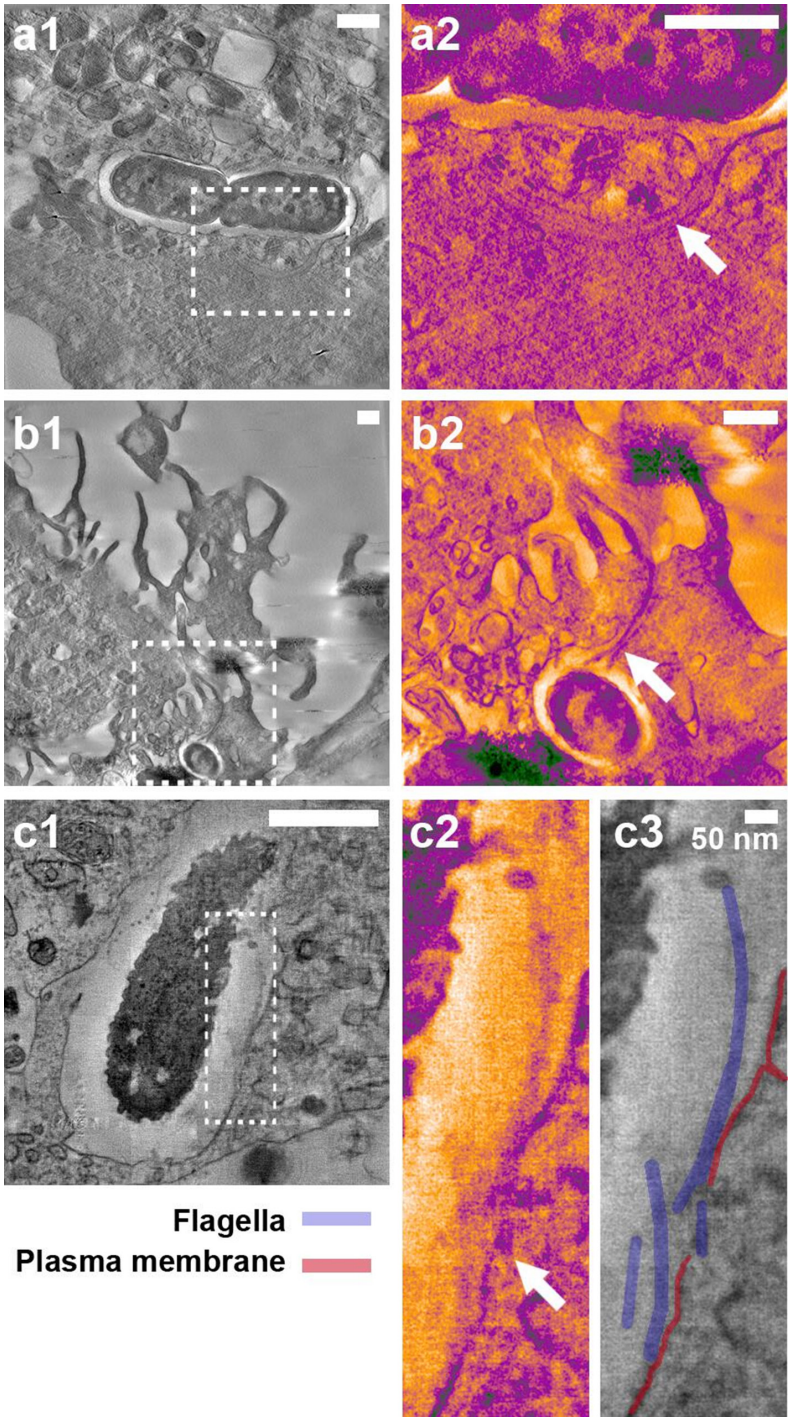

Fig. 5. Electron tomography of host cell membranes in proximity to *S.* Typhimurium flagella-like structures. *S.* Typhimurium SL1344::pAJR145 interacting with IPEC-J2 cells 20 min post-infection. Fixation with 4% (w/v) paraformaldehyde was undertaken for >20 min prior to flagella labelling and samples were not treated with any detergents. Confocal microscopy was used to locate bacteria with flagella in contact with host cells and correlative electron tomography was undertaken (see the Methods section). The contrast of insets was enhanced using the blue_orange_ICB look-up table in Fiji software. (a1) Flagellated *S.* Typhimurium within an epithelial cell. (a2) Inset in (a1); the flagella cross the gross vacuole boundary but are present inside an intact membrane channel (arrow). (b1) Flagellated *S.* Typhimurium inside a membrane ruffle. (b2) Inset in (b1); the flagella bundle passes through the gross boundaries of the ruffle but is adjacent to a distinct membrane boundary (arrow). (c1) Flagellated *S.* Typhimurium at the point of induced uptake into an epithelial cell. (c2) Inset in (c1); flagella in proximity to the disrupted epithelial plasma membrane (arrow). (c3) Structures in (c2) are labelled for clarity. Scale bars, 500 nm unless indicated otherwise.

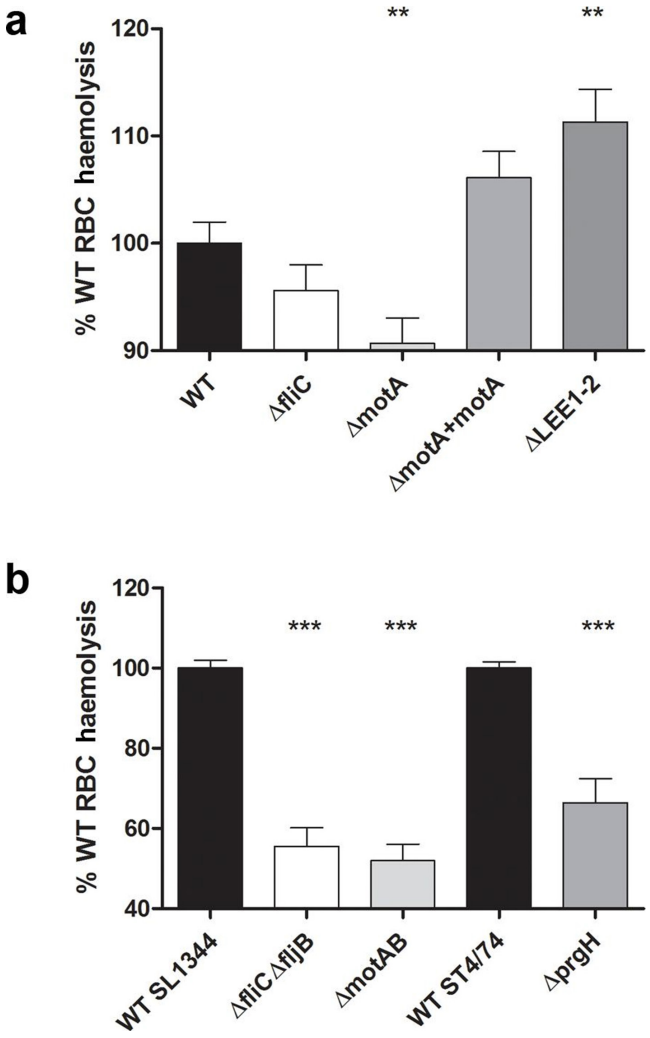

Fig. 6. Contribution of flagella rotation to membrane disruption by *S.* Typhimurium and *E. coli* O157:H7. Sheep RBCs were incubated with stationary-phase cultures of the *E. coli* O157:H7 (a) and *S.* Typhimurium (b) strains indicated for 2 h at 37 °C after centrifugation together at 2000 **g** for 5 min to ensure contact. After incubation, samples were centrifuged at 2000 **g** for 10 min and the A_{405} of supernatants was measured. Data from three to five biological replicates are presented as % wild-type (WT) haemolysis and statistical analysis was performed on raw data using two-tailed homoscedastic Student's *t*-tests; $P \leq 0.01$ (**), $P \leq 0.001$ (***). The results were considered to be significant for a *P* value ≤0.05.

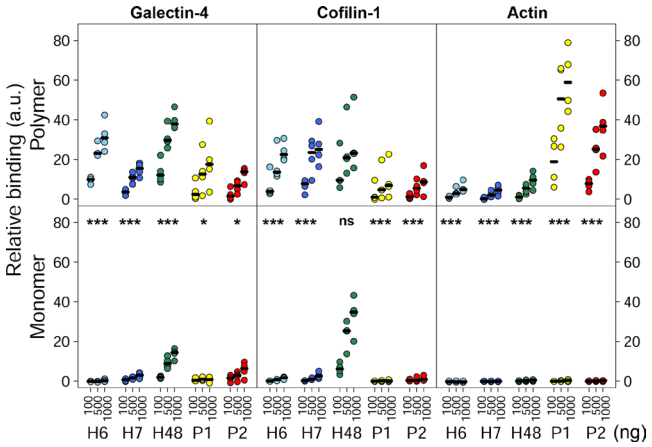

Fig. 7. Relative binding of flagella from *E. coli* and *S.* Typhimurium to identified cellular components, assessed by far ELISA. Binding of 100, 500 and 1000 ng/well of polymeric and monomeric H6 (light blue), H7 (dark blue) and H48 flagella (green) from *E. coli*, and P1 (yellow) or P2 (red) flagella from *S.* Typhimurium to 1000 ng/well galectin-4, cofilin-1 and $\beta\gamma$-actin. Median values of four independent experiments are indicated with black horizontal lines. Relative binding levels are shown as data are normalized to positive and negative detection controls for each antibody and protein pair (see the Methods section). The statistical analyses presented are pairwise comparisons of polymer and monomer using linear mixed effects models. NS, not significant; $P \leq 0.01$ (*), $P \leq 0.0001$(***).

two different concentrations of CFL1 (Fig. 8c). Without CFL1, 250 nM of each flagella type was sufficient to cause a statistically significant increase in the V_{max} of actin polymerization, with *S.* Typhiumurium P2 flagella being the most effective. This low concentration of flagella was chosen to allow detection of increases in actin polymerization rates that may occur as a result of synergy between flagella and CFL1 interactions. Adding an equimolar concentration of CFL1 (250 nM) caused a trend towards further enhanced rates of actin polymerization, but this was not statistically different to addition of CFL1 alone for any of the flagella types tested (P=0.124–0.856). At a 2:1 molar concentration of CFL1:flagella, at which the CFL1 concentration was optimal, further increases in the V_{max} of actin polymerization were apparent for all flagella tested. These increases were only statistically significant with P1 and P2 flagella, compared to the effect of CFL1 alone (P=0.035 and 0.004 respectively). Additionally, there was no statistically significant interaction between CFL1 concentration and flagella type (P=0.6 see the Methods section), indicating that the effects on V_{max} were additive and not due to any synergistic effects of flagella and CFL1 on actin polymerization.

DISCUSSION

We have known for some time now that bacterial flagella are more than just motility organelles. The idea of flagella as long adherence multi-protein complexes for early host surface attachment by commensal and pathogenic bacteria alike is now widely accepted. This raises the question of why there are so few published examples of specific cell-surface protein receptors for flagella.

This paper presents the masking of *Salmonella* and *E. coli* flagella antigens by a detergent-sensitive component, which indicates very intimate interactions of these flagella with host cell lipids. Such a close interaction between flagella and membranes was borne out by confocal microscopy of membrane labelled samples. Additionally, flagella of *S.* Typhimurium and *E. coli* O157:H7 have been shown to bind to cholesterol and ionic sulpho- and phospho-lipids *in vitro*,

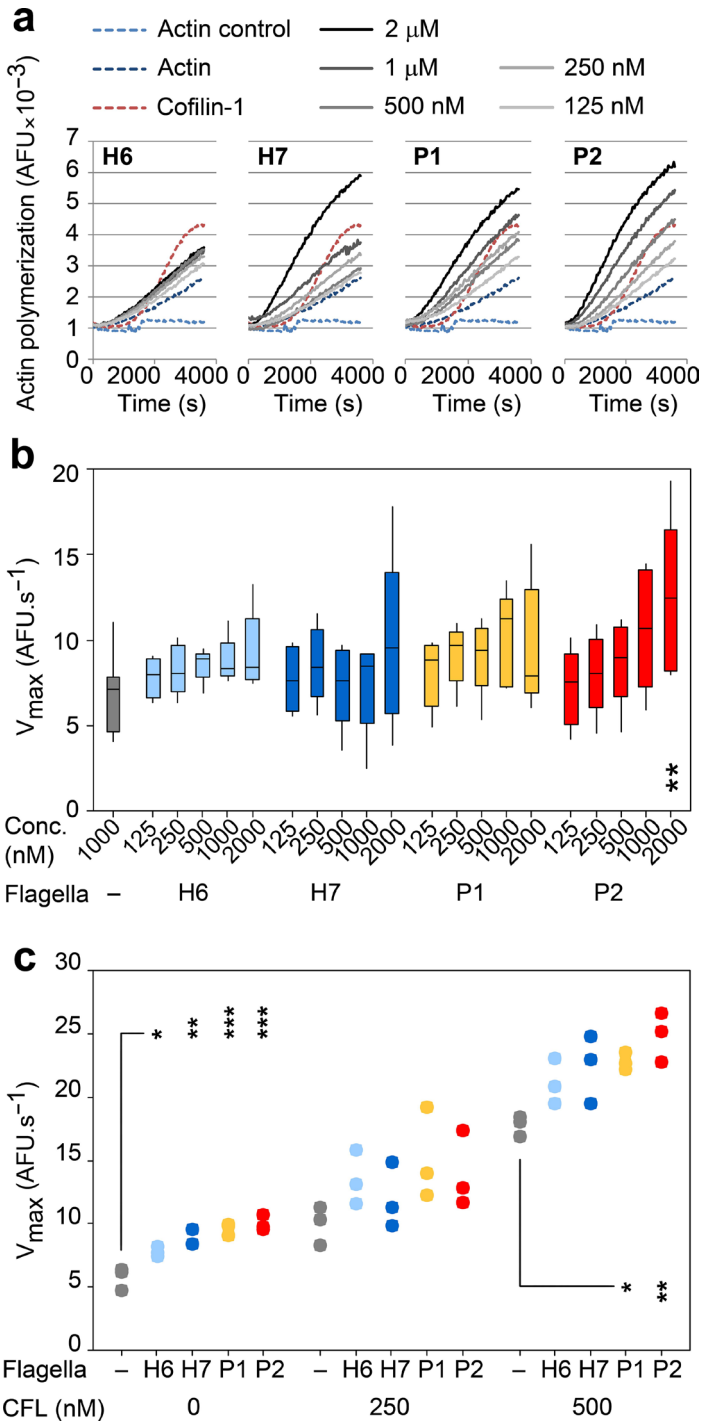

Fig. 8. Impact of flagella type on actin polymerization kinetics. (a) Effects of H6, H7, P1 and P2 flagella on $\alpha\beta$-actin polymerization. Pyrene-conjugated globular (g)-actin polymerization was triggered by the addition of 5 mM KCl, 0.2 mM $MgCl_2$ and 0.1 mM ATP in the presence of different concentrations of flagella, and arbitrary fluorescence (AFU) was measured every 30 s for 1 h at RT. 500 nM cofilin-1 (CFL) was used as a positive control for increased actin polymerization rates in sub-optimal conditions [42]. Data shown are a representative experiment. (b) Maximum velocity (V_{max}) of actin polymerization in the presence of titrating concentrations (125 nM–2 µm) of H6 (light blue), H7 (dark blue), P1 (yellow) and P2 (red) flagella. Data were analysed from five independent experiments and post-hoc Tukey pairwise comparisons of differences between specific flagella concentrations and actin alone are presented; $P<0.01$ (**). (c) V_{max} of actin polymerization in the presence of 250 nM H6, H7, P1 and P2 flagella, and sub-optimal (250 nM) and optimal (500 nM) concentrations of cofilin-1 (CFL). Data represent the results from three independent experiments and post-hoc Tukey pairwise comparisons of the difference between CFL with and without different types of flagella are presented; $P<0.05$ (*), $P\leq0.01$ (**), $P\leq0.001$ (***).

respectively [28, 47], so it is conceivable that these flagella could be binding directly to plasma membranes.

Several studies attribute flagella-mediated adherence to surfaces as largely biophysical processes. It has been demonstrated that *E. coli* H48 flagella are generally attracted to hydrophobic surfaces and are 10 times more likely than the bacterial cell body to make contact with artificial surfaces. These collisions by flagella with hydrophobic abiotic surfaces are known to slow bacteria down, promoting adhesion [48, 49]. This is also true in near-surface swimming, a biophysical process dependent on rotating flagella, which has been shown to aid cooperative colonization by probing and facilitating docking at membrane protrusions [50, 51]. Additionally, the structural properties of different flagellin phase types have been shown to alter *S.* Typhimurium flagella rotation and near-surface swimming behaviour, with downstream effects on colonization [17].

The observations of flagella crossing gross cellular boundaries presented here raise the possibility that flagella-mediated adherence may go beyond surface adhesion. This was routinely detected by confocal microscopy of actin- and membrane-labelled samples. Such overlaps could be explained by insufficient resolution of cellular boundaries, and electron tomography showed this to be at least partially the case. Flagella bundles attached to colonizing bacteria were observed crossing gross cellular boundaries, but the majority remained enclosed within deformed membrane channels. This hints that biophysical membrane deformation by flagella may enhance host membrane ruffling, aiding flagella-dependent adherence by creating favourable surface topologies for membrane binding. Where possible membrane disruption was observed, cells were fixed for microscopy, so there is the potential for observation artefacts resulting from sample dehydration. Freeze fracture and cryo-electron microscopy approaches may provide more definitive answers about the position of flagella in relation to host membranes. However, at the time of writing, the technology to obtain 3D sub-micrometre resolution of moving samples, labelled in a way that will not interfere with interacting surfaces, is not readily available. Nevertheless, the observations are supported by the additional phenotypic data that *E. coli* O157:H7 and *S.* Typhimurium cause 10 and 50%, respectively, less disruption of biological membranes without flagella rotation, compared to wild-type. It is appreciated that these RBC lysis experiments are under conditions where there is high ratio of flagellated bacteria to RBCs and such 'overload' activity is unlikely to be reproduced *in vivo*.

Where potential disruption of host cell membranes in proximity to bacterial flagella was observed by electron tomography, the mechanism by which they do this remains speculative. The haemolysis data support a role for flagella rotation. However, whether this membrane disruption is direct, due to biophysical force, or indirect, due to increased probabilities of favourably charged flagella colliding with membranes, is not known. Alternatively, on epithelial cells this process could be a consequence of pathogen-induced large-scale membrane rearrangements seen during *S.* Typhimurium and *E. coli* O157:H7 colonization, trapping flagella at random, or directed by receptor-mediated endocytosis, triggered by flagella binding to relevant surface molecules. *Pseudomonas aeruginosa* flagella bind to MUC1 and heparin-sulphated proteoglycans and *E. coli* flagella bind to ganglioside receptor GM1 and charged glycerolipids, resulting in immuno-modulation and invasion [28, 52–54]. It is also possible that membrane penetration could be caused by a combination of these factors.

Interaction with actin cytoskeletal proteins was not restricted to flagella from pathogenic bacteria. As established, the predicted surface epitopes of the different polymerized flagellins studied are markedly distinct (Fig. S2), complicating analyses of key surface regions required for CFL1, galectin-4 and βγ-actin binding. Friedlander *et al.* [51] proposed that flagella binding to artificial surfaces involves low-affinity but high-avidity co-operative binding to surface substrates. Multiple low-affinity interactions of the different polymeric flagellins may also account for the direct binding to cytoskeletal proteins observed in the present study. This supports the concept that this co-operative binding of flagellin subunits within a filament is a generic property of flagella. In a pathogenic context this could lend itself to binding repetitive substrates such as actin filaments. Flagella in a non-pathogenic context may be capable of binding to actin and actin-binding proteins, but for this to be relevant, the flagella would have to gain access through the mucus layer to the epithelial surface. Conversely, motility- and flagella-deficient strains of *E. coli* and *S.* Typhimurium can still be pathogenic [55, 56]. However, where expressed, the importance of flagella in the colonization of enteropathogenic and enterohaemorrhagic *E. coli,* and *S.* Typhimurium has been established [17, 24, 30, 57], and this study highlights another potential reason for this.

Furthermore, a recent paper has identified a proteolytic site in the hypervariable region of flagella, present in at least 74 bacterial species, including several species of *Clostridium*. This metallopeptidase domain, named flagellinolysin, was not found in either *E. coli* or *S. enterica* [58]. However, this raises the possibility that these flagella are capable of other enzymatic activities against actin or membrane lipids. Additionally, by using flagellinolysin-negative species, this study could serve as a baseline in assessing the relative contribution of flagellinolysin to flagella-dependent colonization processes in the future.

Flagella interactions with actin were undertaken with isolated components in physiological conditions, confirming direct binding. Many pathogens reorganize host actin architecture during host colonization. The first bacteria described to use actin rearrangement were the intracellular bacteria *Listeria monocytogenes* and *Shigella flexneri* [59, 60]. They both generate filamentous actin 'comet tails' that propel the bacteria through the cytosol, allowing colonization of neighbouring cells. Modulation of actin and actin binding proteins, such as Arp2/3 and CFL1, has also been described for certain pathogenic *E. coli* and *Salmonella* spp. secreted effector proteins

[61, 62]. However, the findings in this current study provide the first evidence of potential actin manipulation by bacterial flagella.

That flagella may be able to plug into this complex system by themselves in standard conditions is intriguing, given the lifestyles of their associated pathogens. For *E. coli* O157:H7, it has been recently shown that the T3SS can be activated by physical forces acting on the bacterium through uncoupling of GrlA/R binding [63] and it is interesting to speculate that flagella surface interactions with membranes could lead to such activation. Cofilin binding by flagella could stabilize F-actin at the site of colonization, setting up the process of intimate attachment that requires T3SS translocation of specific effector proteins [64]. We note that there was no evidence in this study that the *in vitro* binding interactions of H7 flagella with CFL1 affected actin polymerization synergistically. It is possible that additional factors are required for this; if flagella can gain access to the host cytosol directly, the presence of other actin regulators and different micro-environments may inhibit or enhance these interactions to affect host cell binding. For *S.* Typhimurium, recent work has shown how methylation of flagella enhances membrane interactions that promote invasion [65] and subsequent interactions of flagella with actin could contribute to the dynamic regulation of actin by T3SS effectors that enable bacterial invasion [22]. Counter to these pro-infection concepts, intracellular flagella are activators of innate responses via the NLRC4 inflammasome [11, 12] and *S.* Typhimurium flagella activation of NLRC4 is known to induce actin-dependent host cell surface stiffening to prevent further bacterial invasion in macrophages [66].

In summary, the results of this study demonstrate that *S.* Typhimurium and *E. coli* O157:H7 flagella become intimately associated with host cell membranes during initial adherence. This association either results in or is a consequence of host membrane deformation that may cause disruption, with any disruption likely to be a consequence of flagella rotation. *S.* Typhimurium and *E. coli* O157:H7 flagella can bind to actin and actin-binding proteins. These interactions can influence cytoskeletal dynamics *in vitro* and this may be relevant during bacterial colonization. An understanding of how connected these two phenomena are will require further work to elucidate the molecular mechanisms involved.

Funding information
We would like to acknowledge funding from the BBSRC (BB/I011625/1, BBS/E/D/20231761 and BBS/E/D/20002173), as well as a CASE PhD studentship from BBSRC to E. B. W.

Acknowledgements
This paper is dedicated to the memory of Trudi Gillespie. We would like to thank Sutherland Maciver (Edinburgh) for advice on cofilin-1, Kevin Mclean at the Moredun Research Institute proteomics facility for peptide mass fingerprinting, Mike Shipston (Edinburgh) for supplying the STREX-GFP construct, and Phillip Aldridge (Newcastle), Roberto La Ragione (Surrey) and Mark Jepson (Bristol) for supplying reagents and strains, and the Centre for Integrative Physiology (University of Edinburgh) and Wolfson Bioimaging Facility (University of Bristol). We would also like to thank Ian Thompson for his advice and support over the last decade.

Author contributions
E.B.W., Y.R., A.C.G., J.S., P.V., A.B., A.M. and D.L.G. conceived and designed analyses resented in this paper. E.B.W., J.E., A.T., T.G., J.M., S.P.M., E.P., F.L., P.V. and A.M. were involved in carrying out experiments. E.B.W., J.E., A.T., T.G., J.M., Y.R., S.P.M., J.S., P.V., A.B., A.M. and D.L.G. were responsible for analysing data. E.B.W., Y.R. and D.L.G. were responsible for writing the manuscript.

Conflicts of interest
The authors declare that there are no conflicts of interest.

References

1. Chaban B, Hughes HV, Beeby M. The flagellum in bacterial pathogens: for motility and a whole lot more. *Semin Cell Dev Biol* 2015;46:91–103.
2. Berg HC, Anderson RA. Bacteria swim by rotating their flagellar filaments. *Nature* 1973;245:380–382.
3. Chevance FFV, Hughes KT. Coordinating assembly of a bacterial macromolecular machine. *Nat Rev Microbiol* 2008;6:455–465.
4. Berg HC. The rotary motor of bacterial flagella. *Annu Rev Biochem* 2003;72:19–54.
5. Büttner D. Protein export according to schedule: architecture, assembly, and regulation of type III secretion systems from plant- and animal-pathogenic bacteria. *Microbiol Mol Biol Rev* 2012;76:262–310.
6. Diepold A, Armitage JP. Type III secretion systems: the bacterial flagellum and the injectisome. *Philos Trans R Soc Lond B Biol Sci* 2015;370:20150020.
7. Vonderviszt F, Uedaira H, Kidokoro S, Namba K. Structural organization of flagellin. *J Mol Biol* 1990;214:97–104.
8. Zieg J, Silverman M, Hilmen M, Simon M. Recombinational switch for gene expression. *Science* 1977;196:170–172.
9. Yonekura K, Maki-Yonekura S, Namba K. Complete atomic model of the bacterial flagellar filament by electron cryomicroscopy. *Nature* 2003;424:643–650.
10. Hayashi F, Smith KD, Ozinsky A, Hawn TR, Yi EC *et al*. The innate immune response to bacterial flagellin is mediated by Toll-like receptor 5. *Nature* 2001;410:1099–1103.
11. Zhao Y, Yang J, Shi J, Gong Y-N, Lu Q *et al*. The NLRC4 inflammasome receptors for bacterial flagellin and type III secretion apparatus. *Nature* 2011;477:596–600.
12. Miao EA, Andersen-Nissen E, Warren SE, Aderem A. TLR5 and Ipaf: dual sensors of bacterial flagellin in the innate immune system. *Semin Immunopathol* 2007;29:275–288.
13. Yoon S-il, Kurnasov O, Natarajan V, Hong M, Gudkov AV *et al*. Structural basis of TLR5-flagellin recognition and signaling. *Science* 2012;335:859–864.
14. Belas R. Biofilms, flagella, and mechanosensing of surfaces by bacteria. *Trends Microbiol* 2014;22:517–527.
15. Song F, Brasch ME, Wang H, Henderson JH, Sauer K *et al*. How bacteria respond to material stiffness during attachment: a role of *Escherichia coli* flagellar motility. *ACS Appl Mater Interfaces* 2017;9:22176–22184.
16. Floyd M, Winn M, Cullen C, Sil P, Chassaing B *et al*. Swimming motility mediates the formation of neutrophil extracellular traps induced by flagellated *Pseudomonas aeruginosa*. *PLoS Pathog* 2016;12:e1005987.
17. Horstmann JA, Zschieschang E, Truschel T, de Diego J, Lunelli M *et al*. Flagellin phase-dependent swimming on epithelial cell surfaces contributes to productive *Salmonella* gut colonisation. *Cell Microbiol* 2017;19:e12739.
18. Pallen MJ, Matzke NJ. From the origin of species to the origin of bacterial flagella. *Nat Rev Microbiol* 2006;4:784–790.
19. Knutton S, Baldwin T, Williams PH, McNeish AS. Actin accumulation at sites of bacterial adhesion to tissue culture cells: basis of a new diagnostic test for enteropathogenic and enterohemorrhagic *Escherichia coli*. *Infect Immun* 1989;57:1290–1298.

20. Goosney DL, Celli J, Kenny B, Finlay BB. Enteropathogenic *Escherichia coli* inhibits phagocytosis. *Infect Immun* 1999;67:490–495.
21. Hayward RD, Leong JM, Koronakis V, Campellone KG. Exploiting pathogenic *Escherichia coli* to model transmembrane receptor signalling. *Nat Rev Microbiol* 2006;4:358–370.
22. Hume PJ, Singh V, Davidson AC, Koronakis V. Swiss army pathogen: The *Salmonella* entry toolkit. *Front Cell Infect Microbiol* 2017;7:LK.
23. De Souza Santos M, Orth K. The role of the Type III secretion system in the intracellular lifestyle of enteric pathogens. *Microbiol Spectr* 2019;7.
24. Mahajan A, Currie CG, Mackie S, Tree J, McAteer S *et al*. An investigation of the expression and adhesin function of H7 flagella in the interaction of *Escherichia coli* O157:H7 with bovine intestinal epithelium. *Cell Microbiol* 2009;11:121–137.
25. Dziva F, van Diemen PM, Stevens MP, Smith AJ, Wallis TS. Identification of *Escherichia coli* O157:H7 genes influencing colonization of the bovine gastrointestinal tract using signature-tagged mutagenesis. *Microbiology* 2004;150:3631–3645.
26. Naylor SW, Gally DL, Low JC. Enterohaemorrhagic *E. coli* in veterinary medicine. *Int J Med Microbiol* 2005;295:419–441.
27. Erdem AL, Avelino F, Xicohtencatl-Cortes J, Girón JA. Host protein binding and adhesive properties of H6 and H7 flagella of attaching and effacing *Escherichia coli*. *J Bacteriol* 2007;189:7426–7435.
28. Rossez Y, Holmes A, Wolfson EB, Gally DL, Mahajan A *et al*. Flagella interact with ionic plant lipids to mediate adherence of pathogenic *Escherichia coli* to fresh produce plants. *Environ Microbiol* 2014;16:2181–2195.
29. Velge P, Wiedemann A, Rosselin M, Abed N, Boumart Z *et al*. Multiplicity of *Salmonella* entry mechanisms, a new paradigm for *Salmonella* pathogenesis. *Microbiologyopen* 2012;1:243–258.
30. Olsen JE, Hoegh-Andersen KH, Casadesús J, Rosenkranzt J, Chadfield MS *et al*. The role of flagella and chemotaxis genes in host pathogen interaction of the host adapted *Salmonella enterica* serovar Dublin compared to the broad host range serovar *S*. typhimurium. *BMC Microbiol* 2013;13:67.
31. Agbor TA, McCormick BA. Salmonella effectors: important players modulating host cell function during infection. *Cell Microbiol* 2011;13:1858–1869.
32. Rossez Y, Wolfson EB, Holmes A, Gally DL, Holden NJ. *Bacterial flagella*: twist and stick, or dodge across the kingdoms. *PLoS Pathog* 2015;11:e1004483.
33. Blomfield IC, Vaughn V, Rest RF, Eisenstein BI. Allelic exchange in *Escherichia coli* using the Bacillus subtilis sacB gene and a temperature-sensitive pSC101 replicon. *Mol Microbiol* 1991;5:1447–1457.
34. Montie TC, Stover GB. Isolation and characterization of flagellar preparations from *Pseudomonas* species. *J Clin Microbiol* 1983;18:452–456.
35. Smith KD, Andersen-Nissen E, Hayashi F, Strobe K, Bergman MA *et al*. Toll-Like receptor 5 recognizes a conserved site on flagellin required for protofilament formation and bacterial motility. *Nat Immunol* 2003;4:1247–1253.
36. Schierack P, Nordhoff M, Pollmann M, Weyrauch KD, Amasheh S *et al*. Characterization of a porcine intestinal epithelial cell line for *in vitro* studies of microbial pathogenesis in swine. *Histochem Cell Biol* 2006;125:293–305.
37. Mahajan A, Naylor S, Mills AD, Low JC, Mackellar A *et al*. Phenotypic and functional characterisation of follicle-associated epithelium of rectal lymphoid tissue. *Cell Tissue Res* 2005;321:365–374.
38. Wright CS. Structural comparison of the two distinct sugar binding sites in wheat germ agglutinin isolectin II. *J Mol Biol* 1984;178:91–104.
39. Tian L, Jeffries O, McClafferty H, Molyvdas A, Rowe ICM *et al*. Palmitoylation gates phosphorylation-dependent regulation of BK potassium channels. *Proc Natl Acad Sci U S A* 2008;105:21006–21011.
40. Olmos Y, Hodgson L, Mantell J, Verkade P, Carlton JG. ESCRT-III controls nuclear envelope reformation. *Nature* 2015;522:236–239.
41. Sitthidet C, Korbsrisate S, Layton AN, Field TR, Stevens MP *et al*. Identification of motifs of *Burkholderia pseudomallei* BimA required for intracellular motility, actin binding, and actin polymerization. *J Bacteriol* 2011;193:1901–1910.
42. Van Troys M, Huyck L, Leyman S, Dhaese S, Vandekerkhove J *et al*. Ins and outs of ADF/cofilin activity and regulation. *Eur J Cell Biol* 2008;87:649–667.
43. Chattopadhyay S, Moldovan R, Yeung C, XL W. Swimming efficiency of bacterium. *Proc Natl Acad Sci USA* 2006;103:13712–13717.
44. Magariyama Y, Sugiyama S, Kudo S. Bacterial swimming speed and rotation rate of bundled flagella. *FEMS Microbiol Lett* 2001;199:125–129.
45. Parish CR, Wistar R, Ada GL. Cleavage of bacterial flagellin with cyanogen bromide. antigenic properties of the protein fragments. *Biochem J* 1969;113:501–506.
46. Carlsson AE. Stimulation of actin polymerization by filament severing. *Biophys J* 2006;90:413–422.
47. Crawford RW, Reeve KE, Gunn JS. Flagellated but not hyperfimbriated *Salmonella enterica* serovar Typhimurium attaches to and forms biofilms on cholesterol-coated surfaces. *J Bacteriol* 2010;192:2981–2990.
48. Friedlander RS, Vogel N, Aizenberg J. Role of flagella in adhesion of *Escherichia coli* to abiotic surfaces. *Langmuir* 2015;31:6137–6144.
49. Qi M, Gong X, Wu B, Zhang G. Landing dynamics of swimming bacteria on a polymeric surface: effect of surface properties. *Langmuir* 2017;33:3525–3533.
50. Misselwitz B, Barrett N, Kreibich S, Vonaesch P, Andritschke D *et al*. Near surface swimming of *Salmonella* Typhimurium explains target-site selection and cooperative invasion. *PLoS Pathog* 2012;8:e1002810.
51. Friedlander RS, Vlamakis H, Kim P, Khan M, Kolter R *et al*. Bacterial flagella explore microscale hummocks and hollows to increase adhesion. *Proc Natl Acad Sci U S A* 2013;110:5624–5629.
52. Bucior I, Pielage JF, Engel JN. *Pseudomonas aeruginosa* pili and flagella mediate distinct binding and signaling events at the apical and basolateral surface of airway epithelium. *PLoS Pathog* 2012;8:e1002616.
53. Lillehoj EP, Kim BT, Kim KC. Identification of *Pseudomonas aeruginosa* flagellin as an adhesin for Muc1 mucin. *Am J Physiol Lung Cell Mol Physiol* 2002;282:L751–L756.
54. Kato K, Lillehoj EP, Park YS, Umehara T, Hoffman NE *et al*. Membrane-Tethered MUC1 mucin is phosphorylated by epidermal growth factor receptor in airway epithelial cells and associates with TLR5 to inhibit recruitment of MyD88. *J Immunol* 2012;188:2014–2022.
55. Schmitt CK, Ikeda JS, Darnell SC, Watson PR, Bispham J *et al*. Absence of all components of the flagellar export and synthesis machinery differentially alters virulence of *Salmonella enterica* serovar Typhimurium in models of typhoid fever, survival in macrophages, tissue culture invasiveness, and calf enterocolitis. *Infect Immun* 2001;69:5619–5625.
56. Mellmann A, Bielaszewska M, Köck R, Friedrich AW, Fruth A *et al*. Analysis of collection of hemolytic uremic syndrome-associated enterohemorrhagic *Escherichia coli*. *Emerg Infect Dis* 2008;14:1287–1290.
57. Girón JA, Torres AG, Freer E, Kaper JB. The flagella of enteropathogenic *Escherichia coli* mediate adherence to epithelial cells. *Mol Microbiol* 2002;44:361–379.
58. Eckhard U, Bandukwala H, Mansfield MJ, Marino G, Cheng J *et al*. Discovery of a proteolytic flagellin family in diverse bacterial phyla that assembles enzymatically active flagella. *Nat Commun* 2017;8:521.
59. Tilney LG, Portnoy DA. Actin filaments and the growth, movement, and spread of the intracellular bacterial parasite, *Listeria monocytogenes*. *J Cell Biol* 1989;109:1597–1608.

60. Gouin E, Gantelet H, Egile C, Lasa I, Ohayon H *et al*. A comparative study of the actin-based motilities of the pathogenic bacteria *Listeria monocytogenes*, *Shigella flexneri* and *Rickettsia conorii*. *J Cell Sci* 1999;112:1697–1708.
61. Patel JC, Galán JE. Manipulation of the host actin cytoskeleton by *Salmonella*--all in the name of entry. *Curr Opin Microbiol* 2005;8:10–15.
62. Caron E, Crepin VF, Simpson N, Knutton S, Garmendia J *et al*. Subversion of actin dynamics by EPEC and EHEC. *Curr Opin Microbiol* 2006;9:40–45.
63. Sirisaengtaksin N, Odem MA, Bosserman RE, Flores EM, Krachler AM. The *E. coli* transcription factor GrlA is regulated by subcellular compartmentalization and activated in response to mechanical stimuli. *Proc Natl Acad Sci U S A* 2020;117:9519–9528.
64. Slater SL, Sågfors AM, Pollard DJ, Ruano-Gallego D, Frankel G. The type III secretion system of pathogenic *Escherichia coli*. *Curr Top Microbiol Immunol* 2018;416:51–72.
65. Horstmann JA, Lunelli M, Cazzola H, Heidemann J, Kühne C *et al*. Methylation of *Salmonella Typhimurium* flagella promotes bacterial adhesion and host cell invasion. *Nat Commun* 2020;11:11.
66. Man SM, Ekpenyong A, Tourlomousis P, Achouri S, Cammarota E *et al*. Actin polymerization as a key innate immune effector mechanism to control *Salmonella* infection. *Proc Natl Acad Sci U S A* 2014;111:17588–17593.
67. Campellone KG, Roe AJ, Løbner-Olesen A, Murphy KC, Magoun L *et al*. Increased adherence and actin pedestal formation by dam-deficient enterohaemorrhagic *Escherichia coli* O157:H7. *Mol Microbiol* 2007;63:1468–1481.
68. Iguchi A, Thomson NR, Ogura Y, Saunders D, Ooka T *et al*. Complete genome sequence and comparative genome analysis of enteropathogenic *Escherichia coli* O127:H6 strain E2348/69. *J Bacteriol* 2009;191:347–354.
69. Blattner FR, Plunkett G, Bloch CA, Perna NT, Burland V *et al*. The complete genome sequence of *Escherichia coli* K-12. *Science* 1997;277:1453–1462.
70. Flockhart AF, Tree JJ, Xu X, Karpiyevich M, McAteer SP *et al*. Identification of a novel prophage regulator in *Escherichia coli* controlling the expression of type III secretion. *Mol Microbiol* 2012;83:208–223.
71. Arques JL, Hautefort I, Ivory K, Bertelli E, Regoli M *et al*. *Salmonella* induces flagellin- and MyD88-dependent migration of bacteria-capturing dendritic cells into the gut lumen. *Gastroenterology* 2009;137:579–587.
72. Richardson EJ, Limaye B, Inamdar H, Datta A, Manjari KS *et al*. Genome sequences of *Salmonella enterica* serovar typhimurium, choleraesuis, Dublin and gallinarum strains of well- defined virulence in food-producing animals. *J Bacteriol* 2011;193:3162–3163.
73. Morgan E, Campbell JD, Rowe SC, Bispham J, Stevens MP *et al*. Identification of host-specific colonization factors of *Salmonella enterica* serovar Typhimurium. *Mol Microbiol* 2004;54:994–1010.

Edited by: J. Stülke and H. Strahl